An Observational Analysis of the Relationship between Tropical Cyclone Vortex Tilt, Precipitation Structure, and Intensity Change

MICHAEL S. FISCHER,[a,b] ROBERT F. ROGERS,[b] PAUL D. REASOR,[b] AND JASON P. DUNION[a,b]

[a] *Cooperative Institute for Marine and Atmospheric Studies, University of Miami, Miami, Florida*
[b] *NOAA/OAR/Atlantic Oceanographic and Meteorological Laboratory, Miami, Florida*

(Manuscript received 20 April 2023, in final form 20 October 2023, accepted 26 October 2023)

ABSTRACT: This study uses a recently developed airborne Doppler radar database to explore how vortex misalignment is related to tropical cyclone (TC) precipitation structure and intensity change. It is found that for relatively weak TCs, defined here as storms with a peak 10-m wind of 65 kt (1 kt = 0.51 m s^{-1}) or less, the magnitude of vortex tilt is closely linked to the rate of subsequent TC intensity change, especially over the next 12–36 h. In strong TCs, defined as storms with a peak 10-m wind greater than 65 kt, vortex tilt magnitude is only weakly correlated with TC intensity change. Based on these findings, this study focuses on how vortex tilt is related to TC precipitation structure and intensity change in weak TCs. To illustrate how the TC precipitation structure is related to the magnitude of vortex misalignment, weak TCs are divided into two groups: small-tilt and large-tilt TCs. In large-tilt TCs, storms display a relatively large radius of maximum wind, the precipitation structure is asymmetric, and convection occurs more frequently near the midtropospheric TC center than the lower-tropospheric TC center. Alternatively, small-tilt TCs exhibit a greater areal coverage of precipitation inward of a relatively small radius of maximum wind. Greater rates of TC intensification, including rapid intensification, are shown to occur preferentially for TCs with greater vertical alignment and storms in relatively favorable environments.

SIGNIFICANCE STATEMENT: Accurately predicting tropical cyclone (TC) intensity change is challenging. This is particularly true for storms that undergo rapid intensity changes. Recent numerical modeling studies have suggested that vortex vertical alignment commonly precedes the onset of rapid intensification; however, this consensus is not unanimous. Until now, there has not been a systematic observational analysis of the relationship between vortex misalignment and TC intensity change. This study addresses this gap using a recently developed airborne radar database. We show that the degree of vortex misalignment is a useful predictor for TC intensity change, but primarily for weak storms. In these cases, more aligned TCs exhibit precipitation patterns that favor greater intensification rates. Future work should explore the causes of changes in vortex alignment.

KEYWORDS: Convection; Wind shear; Hurricanes/typhoons; Precipitation; Tropical cyclones; Radars/Radar observations

1. Introduction

Accurate forecasts of tropical cyclone (TC) intensity and track are essential to ensure sufficient time for communities in the path of the storm to take the necessary precautions to mitigate damage imposed by TC-related hazards (Morss et al. 2022). Over the past decades, progress has been made in improving both TC track and intensity forecast skill (DeMaria et al. 2014; Cangialosi et al. 2020). However, TC intensity forecast errors continue to be large for events with rapid intensity changes, including both rapid intensification and weakening (Fischer et al. 2019; Trabing and Bell 2020). Trabing and Bell (2020) found the largest TC intensity forecast errors occur when TCs undergo rapid intensification (RI)[1] in the presence of favorable environmental conditions. They hypothesized that in these cases, processes occurring at vortex and convective scales contribute to significant forecast errors and, thus, a better understanding of TC inner-core dynamics is imperative.

A growing body of literature has emerged in recent years aimed at improving our understanding of the processes that affect the rate of TC intensity change, including RI. These studies have shown the rate of TC intensity change is closely linked to the organization of the convective structure within the core of the storm (e.g., within the innermost 200 km). For example, TCs that undergo RI have more symmetric precipitation structures and a greater azimuthal coverage of precipitation than TCs that intensify at lesser rates in both observational studies (Rogers et al. 2013; Zagrodnik and Jiang 2014; Alvey et al. 2015; Tao and Jiang 2015; Tao et al. 2017; Fischer et al. 2018; Shi and Chen 2021) and numerical simulations (Rios-Berrios et al. 2016; Leighton et al. 2018; Miyamoto and Nolan 2018; Tao and Zhang 2019; Alland et al. 2021a; Fischer et al. 2023). Greater rates of TC intensification have also been linked to an increase in concentrated, vigorous bursts of convection, especially if they are located inward of the storm's radius of maximum wind (Guimond et al. 2010; Rogers et al. 2013;

[1] RI is typically defined as an intensity change episode ≥ the 95th percentile of all overwater intensity change episodes (e.g., Kaplan et al. 2010, 2015).

Corresponding author: Michael S. Fischer, michael.fischer@noaa.gov

DOI: 10.1175/MWR-D-23-0089.1

Guimond et al. 2016; Hazelton et al. 2018; Stevenson et al. 2018; Wadler et al. 2018; Chen et al. 2021).

The kinematic structure of the TC vortex has also been linked to TC intensity change. For instance, through a multicase assessment of airborne Doppler radar analyses, Rogers et al. (2013) found intensifying hurricanes are associated with a ring-like vorticity maximum inward of the radius of maximum wind and less vorticity in the TC outer core compared to hurricanes that maintain a steady intensity. Additionally, they found intensifying hurricanes had a deeper and stronger inflow layer as well as greater azimuthally averaged ascent within the TC eyewall than steady-steady hurricanes. These findings were supported by a subsequent study using airborne Doppler radar vertical profiles, conducted by Zhang et al. (2023), which involved a larger number of cases. The Doppler profile analyses indicated that TCs with a relatively narrow vortex structure in the radial direction tended to intensify at greater rates than broad vortices, consistent with previous studies (Carrasco et al. 2014; Martinez et al. 2017; B.-F. Chen et al. 2018; Tao et al. 2020). Zhang et al. (2023) showed that TCs with a narrow vortex had a deeper and weaker inflow layer outward of the radius of maximum wind than broad vortices, but stronger inflow near the radius of maximum wind as well as stronger and more focused ascent. Other studies have linked the vertical structure of the TC vortex to subsequent intensity change. DesRosiers et al. (2023) used airborne Doppler radar observations to show TC intensity change is related to the height of the TC vortex, as storms that rapidly intensify consistently feature relatively tall vortices.

Another important aspect of the vertical structure of a TC is the vertical misalignment, or tilt, of a vortex. For TCs located in environments with a vertically sheared flow, which is nearly ubiquitous in nature (Nolan and McGauley 2012; Rios-Berrios and Torn 2017), the vortex may become vertically misaligned due to differential advection of the background flow (e.g., Jones 1995; Reasor et al. 2004). The effects of vortex tilt can have significant impacts on both the TC precipitation structure and intensity change. For example, in a balanced framework, where a misaligned, but mature, TC can be viewed as a tilted column of enhanced potential vorticity, the tilted vortex is associated with a cold anomaly in the down-tilt direction, while a warm anomaly exists up-tilt of the TC center (Jones 1995; DeMaria 1996; Jones 2000). These thermal perturbations act to induce an azimuthal wavenumber-1 asymmetry in the vertical velocity field as air flows cyclonically around the TC center along slanted isentropic surfaces (Jones 1995; Boehm and Bell 2021). Observational analyses have corroborated the presence of tilt-related thermal and convective asymmetries (Reasor and Eastin 2012; Reasor et al. 2013; Nguyen et al. 2017; Boehm and Bell 2021).

In relatively weak TCs (e.g., storms below hurricane intensity), however, the TC vortex may not be characterized by a single column of enhanced potential vorticity, but, rather, the TC can feature multiple circulation centers at a given vertical level, which are strongly tied to diabatic processes (e.g., Huntley and Diercks 1981; Reasor et al. 2005; Sippel et al. 2006; Rios-Berrios et al. 2018; Schecter and Menelaou 2020). Furthermore, the vertical structure of vortex misalignment may be discontinuous in nature, with large "jumps" in the location of the primary TC center between vertical levels (e.g., Fischer et al. 2022). Numerical modeling simulations have demonstrated that in these disorganized and misaligned TCs, the balanced temperature perturbations associated with vortex misalignment can limit buoyancy near the lower-tropospheric TC center, with most of the convection occurring near the predominant midtropospheric TC center (e.g., Rios-Berrios et al. 2018; Schecter 2022). These asymmetric convective structures are generally viewed as less favorable for TC intensification than convection distributed symmetrically about the TC center (Nolan and Grasso 2003; Nolan et al. 2007; Schecter and Menelaou 2020; Schecter 2022).

A misaligned vortex can also affect the convective organization of a TC by providing a pathway for low-entropy, environmental air to enter the TC warm core (Davis and Ahijevych 2012; Alland et al. 2021b; Finocchio and Rios-Berrios 2021; Fischer et al. 2023). Intrusions of environmental air can collapse convection in the TC rainband region and flush the TC boundary layer with low-entropy air, which limits the areal coverage and vigor of ascending air parcels (Riemer et al. 2010; Alland et al. 2021a; Chen et al. 2021; Wadler et al. 2021). In some cases, intrusions of low-entropy, environmental air can be radially transported into the midtropospheric TC core, where the buoyancy of convective plumes can be reduced, or even eliminated altogether (Cram et al. 2007; Tang and Emanuel 2010; Alland et al. 2021b; Finocchio and Rios-Berrios 2021; Fischer et al. 2023). In both ventilation pathways, the convective organization of the TC is disrupted and TC intensification is limited.

Consistent with the negative impacts of vortex misalignment on TC intensification, the majority of previous observational case studies (Rogers et al. 2015, 2016, 2020) and numerical modeling studies (Zhang and Tao 2013; Rios-Berrios et al. 2018; Tao and Zhang 2019; Alvey and Hazelton 2022; Schecter 2022) have indicated that in order for more rapid rates of TC intensification to be realized, a TC must be sufficiently vertically aligned. However, this consensus is not unanimous and the degree of alignment required for RI is unclear. For example, Alvey et al. (2022) used airborne and ground radar analyses to show Tropical Storm Dorian (2019) began a period of RI despite some degree of vortex misalignment, hypothesizing alignment can be achieved during periods of intensification. Likewise, some numerical simulations have shown vortex alignment is not required for the onset of RI (Chen and Gopalakrishnan 2015; X. Chen et al. 2018b) and, rather, vortex alignment occurs as the result of RI (Chen and Gopalakrishnan 2015). In a similar vein, Rogers et al. (2013) found that intensifying and steady-state hurricanes had statistically similar magnitudes of vortex tilt using airborne Doppler analyses. Consequently, there is still significant uncertainty in regard to how vortex misalignment is related to TC intensity change and RI. This is especially true for storms observed in nature, as there has yet to be a systematic observational analysis of the relationship between vortex misalignment and TC intensity change that has included TCs below hurricane intensity—an intensity regime where vortex misalignment is frequently large (Fischer et al. 2022).

The goal of the present analysis is to address this gap by performing a comprehensive observational analysis of the relationship between vortex misalignment, TC precipitation structure, and TC intensity change using a recently developed airborne Doppler radar database. By characterizing these relationships, we aim to improve our understanding of how TC intensity

change, including a focus on RI, is linked to aspects of the TC vortex and convective structures. Ultimately, it is our hope that this improved understanding can be utilized to improve TC intensity forecasts.

2. Data and methods

a. Description of datasets

This study examines analyses of three-dimensional TC kinematic structure and radar reflectivity from the Tropical Cyclone Radar Archive of Doppler Analyses with Recentering (TC-RADAR; Fischer et al. 2022). TC-RADAR is a collection of dual-Doppler radar analyses based on observations collected from the X-band tail Doppler radar (TDR) onboard NOAA's WP-3D (P3) aircraft over the last three decades. Analyses in TC-RADAR are available at a horizontal grid spacing of 2.0 km and a vertical grid spacing of 0.5 km for heights of 0.5–18.0 km. Additional details about the TDR system and the radar synthesis process are available in Fischer et al. (2022). While the radar system and quality-control process are the same as that described in Fischer et al. (2022), the present study uses an updated version of TC-RADAR,[2] which contains additional cases from the 2021 and 2022 seasons, as well as an improved TC center-finding procedure. The TCs sampled in TC-RADAR primarily occurred in the North Atlantic basin, with a few cases in the eastern and central North Pacific (Fischer et al. 2022).

TC-RADAR contains analyses in two formats: 1) Individual TDR "swath" analyses, typically associated with a single pass through the center of the TC and, in some cases, a downwind leg[3] through the TC rainband region or 2) "Merged" analyses, which average all TDR swath analyses for a given flight. Because one of the aims of the present study is to investigate how the TC precipitation structure is related to vortex misalignment, it is desirable to calculate misalignment from individual swath analyses to account for cases where the TC vortex tilt and precipitation structure significantly evolve over the duration of a given reconnaissance flight. The previous center-finding method used in Fischer et al. (2022) was designed to identify the TC tilt structure from merged analyses, which typically have greater data coverage than swath analyses. To more reliably identify vortex tilt from individual TDR swath analyses, the TC-RADAR center-finding method was refined. The essence of the center-finding method is similar to the previous version: A TC center is identified as the analysis grid point where the storm-relative flow best matches an idealized vortex of purely cyclonic flow, as determined by a cost function. However, in the updated center-finding method used here, additional data coverage constraints have been implemented and the cost function used to determine the TC center has been slightly modified. The refined TC center-finding method, which we have elected to name the Weighted Circulation Maximization (WCM) method for clarity, is described in more detail in appendix A.

An example of TC centers identified from the WCM method is shown in Fig. 1. Here, four consecutive TDR swath analyses from the 100828I1 P3 mission into Tropical Storm Earl (2010) indicate a cyclonic precession of the 2- and 7-km TC centers about one another. Interestingly, the midlevel (7.0-km) vortex center is consistently located within a region of enhanced reflectivity. This evolution agrees with previous analyses of Earl that identified a cyclonic propagation of convective bursts (Rogers et al. 2015) and lightning activity (Stevenson et al. 2014) during this period. The tilt and precipitation evolution shown in Fig. 1 demonstrates the utility of identifying the TC tilt structure from individual TDR analyses, as a composite of the four analyses would have washed out the details of this evolution.

As seen in Fig. 1, this study also uses satellite infrared (IR) brightness temperatures, which can be a useful proxy for the TC convective structure in locations without TDR observations. 10.3-μm IR brightness temperatures were obtained from NOAA's Merged IR (MERGIR) database (Janowiak et al. 2017), which are available at approximately 4-km horizontal grid spacing every 30 min. Each of the 1021 unique TDR swath analyses in TC-RADAR was paired with IR brightness temperatures from the nearest 30-min observation time, which guaranteed IR brightness temperatures were sampled within 15 min of the TDR analysis time. For a more direct comparison, IR brightness temperatures were interpolated onto the same Cartesian grid coordinates as the corresponding TDR analysis using a cubic interpolation scheme.

b. Bias-correcting TDR reflectivities

This study uses TDR-derived reflectivities to characterize the TC precipitation structure. An inspection of the TC-RADAR database revealed biases in the distribution of TDR reflectivities from year to year, and in some cases, between the TDR systems on each P3 aircraft during the same year. To mitigate these biases and facilitate a more accurate comparison of the observed reflectivities in different years or sampled by different TDR systems, this study employed a reflectivity bias-correction method based on a probability matching technique, similar to that used in Wadler et al. (2023). This process is described in detail in appendix B. Here, we simply note that this study solely uses the bias-corrected TDR reflectivities in all analyses, including those shown in Fig. 1.

c. Quantifying vortex tilt

As shown in Fischer et al. (2022), TCs exhibit a range of vortex misalignment structures, especially when TCs are below hurricane intensity. In an effort to simplify the relationship between vortex misalignment and TC intensity change or precipitation structure, we sought to quantify vortex misalignment using a single metric. Hereafter, tilt magnitude and direction correspond to the magnitude and direction of the largest horizontal displacement vector that exists between the TC center at a height of 2 km and an upper TC center located at a height between 5 and 6.5 km. This tilt metric does not require center estimates to exist at every TDR analysis height

[2] This study used TC-RADAR version v3 k.

[3] A "downwind leg" refers to the portion of the flight track following a radial penetration through the center of the storm. Here, the aircraft flies with the cyclonic flow of the TC, typically beginning at a radius of 165–195 km, to set up the next radial penetration through the center of the TC at a different azimuthal heading.

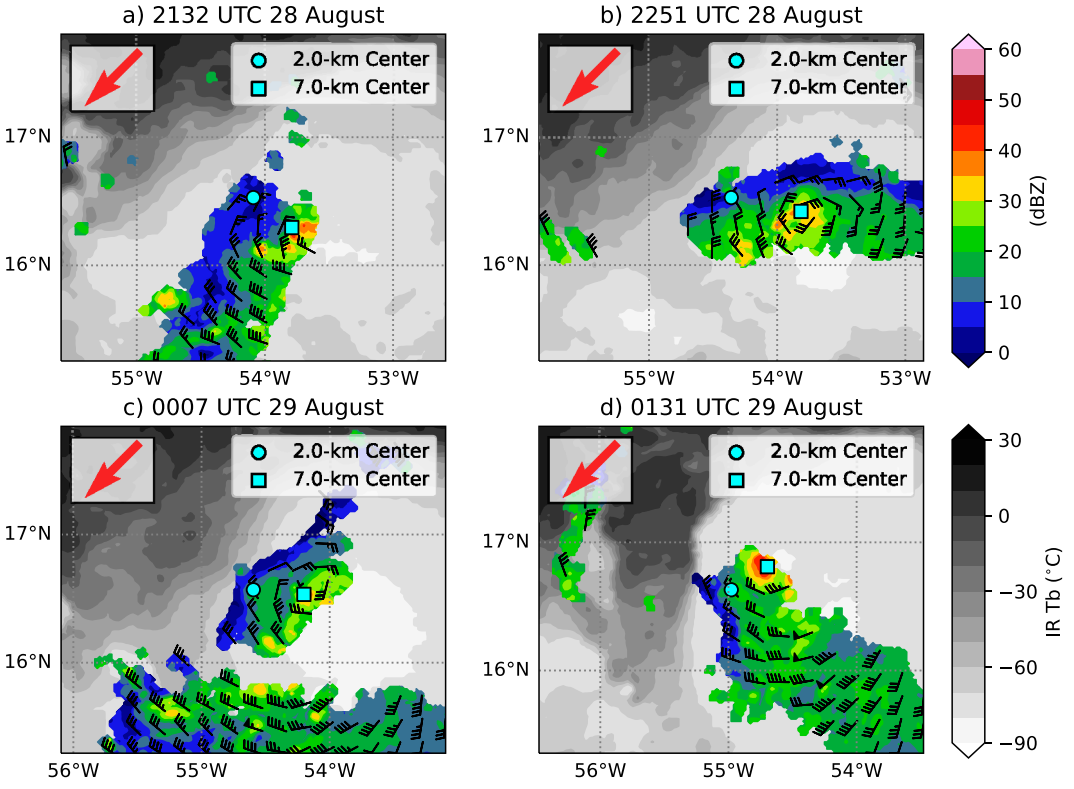

FIG. 1. (a) TDR analyses of reflectivity (shaded; dBZ) and storm-relative wind (barbs; kt) at a height of 7 km for the 100828I1 mission into Tropical Storm Earl. The 2- and 7-km TC centers are denoted by the cyan circle and square, respectively. Analysis is valid at 2132 UTC 28 Aug 2010. Coincident satellite-derived infrared brightness temperatures (°C) are shown in the grayscale shading. The environmental vertical wind shear direction is shown by the red arrow in the top-left inset. (b)–(d) As in (a), but for analyses valid at (b) 2251 UTC 28 Aug, (c) 0007 UTC 29 Aug, and (d) 0131 UTC 29 Aug.

within this layer as some cases have limited data coverage that preclude TC center estimates; however, we do require TC center estimates exist at heights of 2.0 km and at least one height between 5.0 and 6.5 km. Sensitivity tests indicated this tilt metric yielded stronger correlations to future TC intensity change than requiring all TC center estimates exist between the 2- and 6.5-km layer (not shown). The tilt metric used in this study was selected as it maximized the signal between vortex tilt and TC intensity change; however, other vertical layers produced similar patterns (not shown). It is important to acknowledge that the words "tilt" and "misalignment" are used interchangeably in this study. To determine the tilt of a TC vortex, we do not require a coherent column of vorticity to exist. Instead, for the purposes of this study, we are simply interested in how the displacement between a lower-tropospheric and mid-tropospheric TC center are related to TC intensity change and precipitation structure.

In an effort to prevent TCs located in significantly unfavorable thermodynamic environments—which are unlikely to intensify even with favorable vortex structures—from masking a potential signal between TC intensity change and vortex misalignment, this study excluded TDR analyses of storms in environments where the oceanic heat content was below 10 kJ cm^{-2} or the midlevel (i.e., 700–500-hPa) relative humidity was below 40%.[4] Implementing these thresholds removed 87 cases from the overall initial total of 648 TDR analyses where a tilt magnitude could be identified. The following conclusions were not found to be overly sensitive to the precise thresholds used to exclude cases in unfavorable thermodynamic environments (not shown).

The resulting distribution of TC tilt magnitudes are shown in Fig. 2 as a function of TC intensity. Recall that these tilt estimates are derived from individual TDR swath analyses, unlike the results of Fischer et al. (2022), which examined merged TDR analyses. However, similar to the findings of Fischer et al. (2022), Fig. 2 indicates vortex tilt magnitude displays a nonlinear relationship with TC intensity.[5] Strong TCs (hereafter defined as cases with maximum sustained 10-m wind > 65 kt (1 kt $= 0.51$ m s^{-1}) and shown on the right side of the

[4] All environmental fields in this study were determined by developmental data for the Statistical Hurricane Intensity Prediction Scheme (SHIPS; DeMaria and Kaplan 1994; DeMaria et al. 2005).

[5] In this study, all best track intensity estimates and environmental fields were derived from the nearest synoptic time to the time of the TDR analysis, as in Fischer et al. (2022).

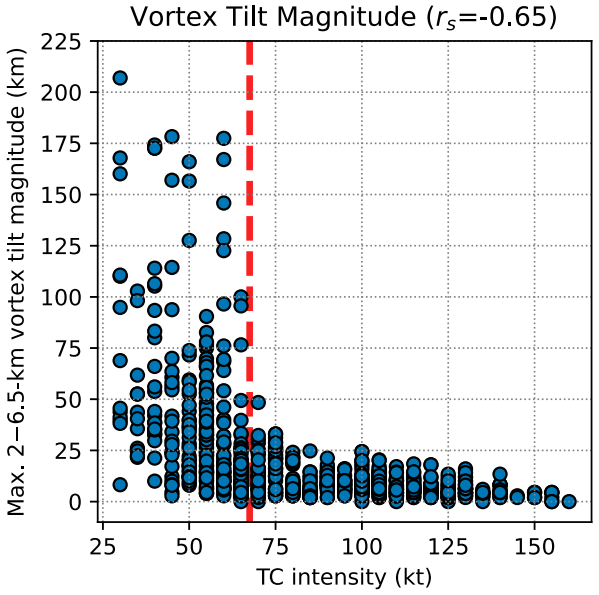

FIG. 2. Scatterplot of the maximum 2–6.5-km vortex tilt magnitude (km), as a function of best track TC intensity (kt). Each point represents a unique TDR analysis. A dashed vertical red line denotes the separation between weak TCs (best track intensity ≤ 65 kt) and strong TCs (best track intensity > 65 kt). The rank correlation coefficient is denoted by r_s.

dashed, vertical, red line in Fig. 2) have tilt magnitudes less than approximately 50 km. Alternatively, weak TCs (hereafter defined as cases with maximum sustained 10-m wind ≤ 65 kt and shown on the left side of the dashed, vertical, red line in Fig. 2) exhibit a wide range of tilt magnitudes, including vortices that are nearly aligned and tilt magnitudes of approximately 200 km.[6] This relationship between tilt magnitude and TC intensity agrees with previous idealized modeling studies, which have shown a reduction in vortex tilt frequently occurs before a developing TC reaches hurricane intensity (Rios-Berrios et al. 2018; Schecter and Menelaou 2020; Rios-Berrios 2020; Schecter 2022). The following sections will explore the relationship between vortex misalignment, TC intensity change and precipitation structure using the set of cases shown in Fig. 2.

3. Results

a. *How is vortex tilt related to TC intensity change?*

A goal of this study is to identify the relationship between vortex misalignment and TC intensity change. However, as shown in Fig. 2, the distribution of vortex tilt depends on the TC intensity. One way to account for the differing distributions of vortex tilt in relation to TC intensity is to group cases into different intensity-based categories. Here, we focus on the two previously defined intensity groups: strong and weak TCs. The relationship between tilt magnitude and future 12-h TC intensity change for all TCs, strong TCs, and weak TCs is shown in Fig. 3. Here we consider 12-h TC intensity change as being representative of a temporal scale responsive to changes in vortex-scale processes, similar to previous analyses of TC intensity change using airborne Doppler radar observations, such as Rogers et al. (2013). The relationship between vortex misalignment and subsequent TC intensity change at differing lag times is explored later in this analysis.

When considering TCs of all intensities, little relationship exists between the magnitude of vortex tilt and TC intensity change (Figs. 3a,d). This is reflected by relatively small rank correlation coefficients between vortex tilt magnitude and TC intensity change (values given by r_s in Fig. 3). Additionally, both tails of the intensity change distribution are associated with tilt magnitudes less than 50 km, indicating nearly aligned vortices are capable of both RI[7] and rapid weakening. TCs experiencing relatively small intensity changes, such as changes in central pressure ≤ 10 hPa or changes in maximum sustained-wind ≤ 10 kt are the cases associated with the largest range of tilt magnitudes.

A signal between vortex tilt magnitude and TC intensity change begins to emerge when also considering TC intensity. For strong TCs, the magnitude of vortex tilt displays a weak, but statistically significant relationship[8] to TC intensity change when TC intensity is defined by the maximum sustained wind (Fig. 3e). Strong TCs that intensify at greater rates tend to display more aligned vortices than strong TCs that weaken, although there is considerable spread in this relationship, as reflected by a rank correlation coefficient of −0.06. When TC intensity change is defined by changes in the TC central pressure, no appreciable relationship is found between vortex misalignment and TC intensity change in strong TCs (Fig. 3b). Because strong TCs are consistently associated with relatively small vortex tilt magnitudes, this may help explain why the smaller sample size examined by Rogers et al. (2013) did not yield significant differences in the magnitude of vortex tilt between intensifying and steady-state hurricanes.

The relationship between vortex misalignment and TC intensity change becomes more apparent in weak TCs (Figs. 3c,f). Although some variability exists, weak TCs that intensify at greater rates tend to have more aligned vortices. The rank correlation coefficient between vortex tilt magnitude and TC intensity change is 0.44 and −0.41, as defined by changes in central pressure and maximum wind speed, respectively. These correlations were found to be statistically significant at the 99.9% confidence level. Interestingly, weak TCs that undergo RI are consistently associated with tilt magnitudes < 30 km (Fig. 3f). The same pattern is also found in strong TCs (Fig. 3e); however, because many TCs have tilt magnitudes < 30 km but do not undergo RI, this result suggests that a relatively aligned vortex may be a necessary, but not sufficient, condition for RI. Although such a

[6] It is possible, if not likely, some TCs in nature have tilt magnitudes in excess of 200–225 km, but due to typical flight patterns and the spatial constraints of the TDR analysis domain, we were not able to identify any such cases.

[7] Defined as a 12-h increase in the maximum sustained 10-m wind ≥ 20 kt, consistent with Kaplan et al. (2015).

[8] In this study, a correlation between two variables was determined to be statistically significant if a two-sided t test yielded a p value < 0.05.

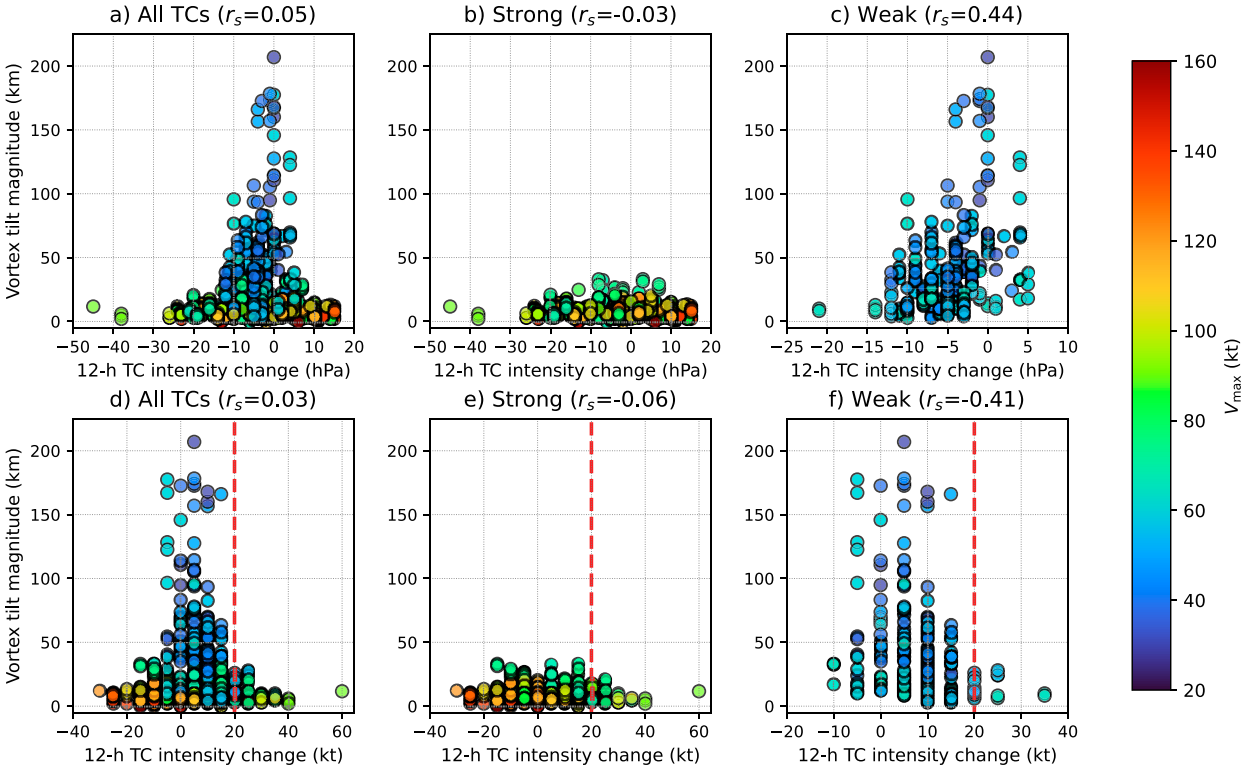

FIG. 3. (a) Scatterplot of the vortex tilt magnitude (km) and the future 12-h change in the TC best track central pressure (hPa). Each point represents a unique TDR analysis, where the color of the marker corresponds to the best track TC intensity (kt). The rank correlation coefficient is denoted by r_s. (b),(c) As in (a), but for strong and weak TCs, respectively. (d)–(f) As in (a)–(c), but for the future 12-h change in the TC best track maximum wind (kt) instead of the central pressure. The 12-h RI threshold (20 kt) is highlighted by the vertical dashed red line.

hypothesis has been provided in previous modeling studies (Tao and Zhang 2014; Alvey et al. 2020; Rios-Berrios 2020; Schecter and Menelaou 2020; Schecter 2022), it is our understanding that this is the first time a multistorm observational analysis has demonstrated RI occurs preferentially for storms with relatively small-tilt magnitudes.

The results presented in Fig. 3 demonstrate the magnitude of vortex tilt is closely related to the rate of TC intensity change in weak TCs over the following 12 h; however, does this relationship hold true for other lead times? To investigate this question, Fig. 4 shows the rank correlation coefficient between vortex tilt magnitude and TC intensity change as a function of the subsequent intensity change duration. For context, the rank correlation coefficient between the deep-layer environmental shear magnitude[9] is also shown as a function of subsequent intensity change duration for the same set of cases where tilt estimates are available. The vertical wind shear magnitude has been used in many statistical models as a robust predictor of TC intensity change (DeMaria and Kaplan 1994, 1999; Emanuel et al. 2004; Knaff et al. 2005; Kaplan et al. 2015). As shown in Fig. 4, the magnitude of vortex tilt has a stronger relationship to TC intensity change than the magnitude of the vertical wind shear for the majority of forecast lead times between 6 and 48 h, when TC intensity change is defined by the TC central pressure, and for forecast lead times over the next 12 h when intensity change is defined by the peak wind. It is unclear why tilt is more strongly correlated to changes in TC central pressure than peak wind, but potential explanations include: 1) the more precise best track intensity intervals for central pressure (1 hPa) than peak wind (5 kt), 2) changes in peak wind speed can also be associated with changes in TC translation speed, 3) TC central pressure may more readily respond to changes in the vertically integrated TC warm core associated with changes in vortex tilt (e.g., Tao and Zhang 2019; DesRosiers et al. 2022), or 4) the difference in the correlation coefficients between peak wind and central pressure result from the noise of a limited sample size. Nevertheless, Fig. 4 indicates the utility of observations of vortex tilt in predicting TC intensity change, particularly at relatively short lead times, where it appears the vortex tilt structure contains additional information on subsequent TC intensity change beyond that provided by the environmental shear magnitude. For simplicity, the remainder of this study will focus on the relationships between vortex misalignment and 12-h TC intensity change.

[9] The shear magnitude is derived from the SHDC parameter in the SHIPS diagnostic file. This shear is defined as the 850–200-hPa difference of the mean wind within 500 km of the TC center after a vortex removal technique is applied.

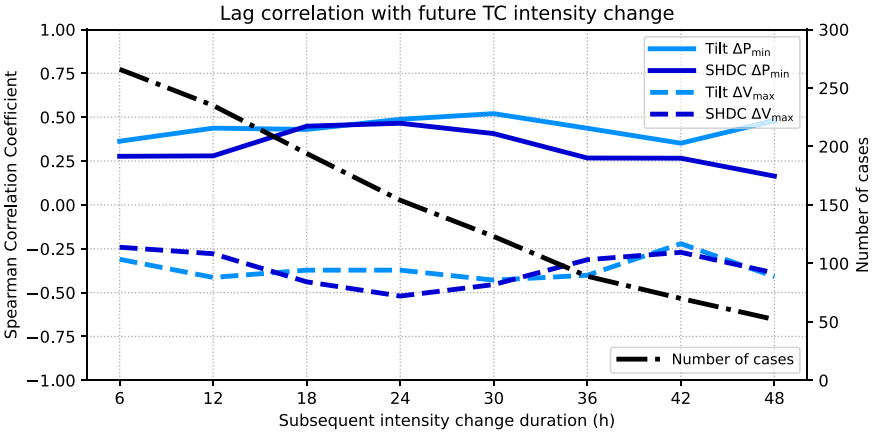

FIG. 4. Spearman rank correlation coefficient between future TC intensity change and tilt magnitude (light blue line) or 850–200-hPa shear magnitude (SHDC; dark blue line). Solid lines define TC intensity change using changes in best track central pressure, whereas dashed lines define TC intensity change using changes in best track maximum 10-m wind. Results are shown as a function of the subsequent TC intensity change duration; however, both the tilt and shear magnitude are only computed at the onset of the intensity change episode. Only weak TCs are considered here. The number of cases considered in each time period is shown by the dot–dashed black line.

In addition to the magnitude of vortex tilt, previous studies have suggested that direction of vortex tilt may be linked to TC intensity change. It has been hypothesized that if the vortex tilt precesses into a location that is upshear-left of the low-level center, this may be a favorable configuration for TC intensification, as a combination of vertical wind shear and diabatic processes may help to align the vortex (Jones 1995; Reasor et al. 2004; Stevenson et al. 2014; Tao and Zhang 2014; Rogers et al. 2015; Rios-Berrios et al. 2018; Ryglicki et al. 2018; Tao and Zhang 2019). To investigate whether TC intensification is preferred for certain shear-relative tilt orientations in nature, Fig. 5 shows the shear-relative tilt location of maximum vortex misalignment for weak TCs, shaded by the future 12-h change in central pressure. We did not identify a systematic preference for TC intensification for certain shear-relative tilt orientations; however, the number of cases with an upshear tilt orientation was small. Instead, the majority of weak TCs display a downshear-left tilt, consistent with the results of Fischer et al. (2022) and previous theoretical work (e.g., Reasor et al. 2004).

Figure 5 suggests that in nature, TC intensity change is more closely related to the tilt magnitude than the shear-relative tilt direction; however, a larger sample size is required to have more confidence in this conclusion. It is also possible that the results presented in Fig. 5 would differ if the shear was computed using a different domain size. For example, Boehm and Bell (2021) found the observed vortex tilt direction in Hurricane Rita (2005) was oriented downshear relative to the large-scale shear, but left-of-shear when the shear was computed within a more local domain, comparable to the spatial scale of the TC inner core. Unfortunately, data coverage gaps, which are especially problematic in weak TCs, prevent us from performing a robust analysis of how vortex misalignment is related to TDR-derived estimates of a local-scale shear. Future work would benefit from a better understanding of how vortex tilt responds to differing spatial scales, and evolutions, of vertical wind shear. For now, the present study will focus on how vortex misalignment is related to the synoptic-scale deep-layer shear derived from SHIPS, which will also facilitate comparisons with previous studies that have used similar shear metrics.

b. *How is vortex tilt related to the TC environment?*

To better understand the relationship between TC intensity change and vortex misalignment, it is useful to explore how vortex misalignment is related to the storm's environment. Figure 6 shows scatterplots of the vortex tilt magnitude in relation to four different metrics of environmental favorability for TC intensification. Figure 6a demonstrates the magnitude of vortex tilt is positively correlated with the magnitude of the deep-layer environmental vertical wind shear. In essence,

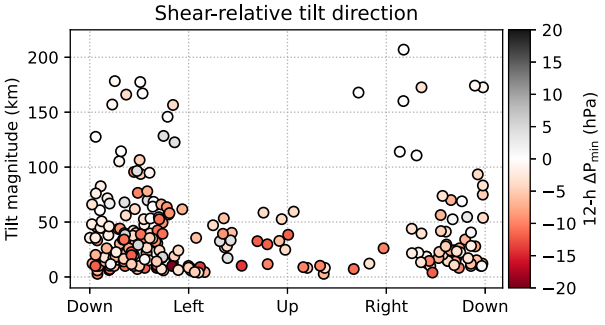

FIG. 5. Scatterplot of the shear-relative tilt direction (indicated by the labels along the abscissa) for weak TCs. Each point represents a unique analysis, where the color of the marker corresponds to the future 12-h change in best track central pressure (ΔP_{min}).

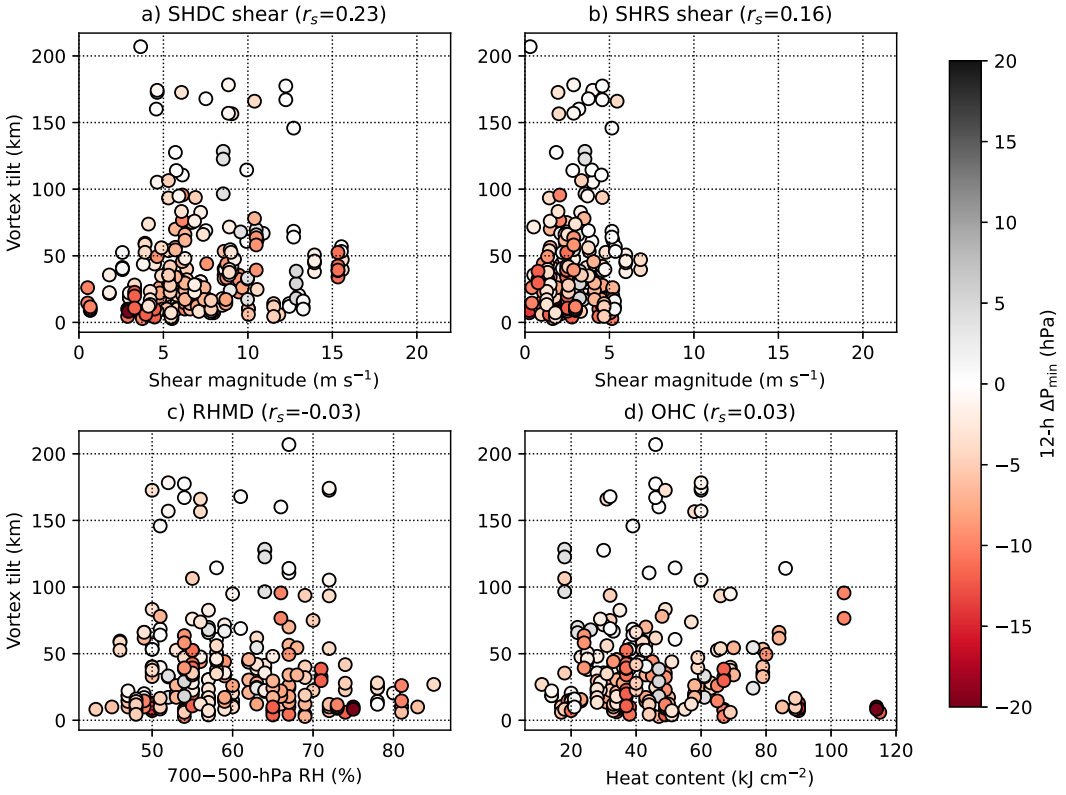

FIG. 6. (a) Scatterplot of the maximum 2–6.5-km vortex tilt magnitude (km) and 850–200-hPa vertical wind shear magnitude (SHDC; m s^{-1}). Each point represents a unique analysis, where the color of the marker corresponds to the future 12-h change in best track central pressure (ΔP_{min}). Here, only weak TCs were analyzed. The rank correlation coefficient is denoted by r_s. Environmental data are derived from the synoptic time closest to the time of the TDR analysis. (b)–(d) As in (a), but for the relationship between tilt magnitude and (b) the 850–500-hPa shear magnitude (SHRS; m s^{-1}), (c) 700–500-hPa layer-averaged relative humidity (RHMD; %) averaged within a 200–800-km TC-centered annulus, and (d) the local oceanic heat content (OHC; kJ cm^{-1}).

smaller values of vertical wind shear favor smaller vortex tilt magnitudes, whereas larger shear magnitudes favor larger vortex tilt magnitudes. While this result is not surprising and consistent with previous theoretical and modeling work (Reasor et al. 2004; Tao and Zhang 2014; Alland et al. 2021a), the amount of variability in the relationship between shear and vortex tilt is intriguing. For instance, some weak TCs are observed to have nearly aligned vortices despite >10 m s^{-1} of shear, whereas some weak TCs display vortex tilt magnitudes > 100 km despite shear magnitudes < 5 m s^{-1}. It is possible some of this variability arises from a lagged response of the TC tilt structure to changes in the magnitude of shear (e.g., Onderlinde and Nolan 2017; Finocchio and Rios-Berrios 2021), which is not considered here. Perhaps the most interesting result from Fig. 6a is that both the deep-layer shear magnitude and the vortex tilt magnitude provide unique information about the likelihood for TC intensification. For example, for a given shear magnitude, TCs are more likely to intensify when the vortex tilt magnitude is small. Likewise, for a given tilt magnitude, TCs are more likely to intensify when the shear magnitude is small.

Idealized simulations have shown that shallower layers of shear, focused lower in the troposphere, cause a vortex to tilt more significantly than shear focused higher in the troposphere (e.g., Finocchio et al. 2016). To investigate whether vortex tilt is more closely related to a measure of midtropospheric shear, Fig. 6b shows the distribution of vortex tilt relative to the 850–500-hPa shear magnitude. Curiously, the relationship between midtropospheric shear and tilt magnitude is significantly weaker than the relationship between deep-layer shear and tilt magnitude shown in Fig. 6a. This result is reminiscent of the findings of Finocchio and Majumdar (2017), who discovered the depth and height of observed shear layers are only weak predictors of TC intensity change compared to the deep-layer shear magnitude. Nevertheless, for a fixed midtropospheric shear magnitude, TCs intensify at greater rates when vortex tilt is small (Fig. 6b).

The magnitude of vortex tilt displayed little relationship to select thermodynamic characteristics of the TC environment, such as midtropospheric relative humidity (Fig. 6c) or oceanic heat content (Fig. 6d). However, the joint relationship between vortex tilt magnitude, environmental favorability, and TC intensity change is still apparent. Specifically, TC intensification occurs preferentially for small-tilt magnitudes, greater relative humidity (Fig. 6c), and higher oceanic heat content (Fig. 6d).

The results shown in Fig. 6 reflect the multiscale nature of TC intensity change. For instance, a given TC may be associated with

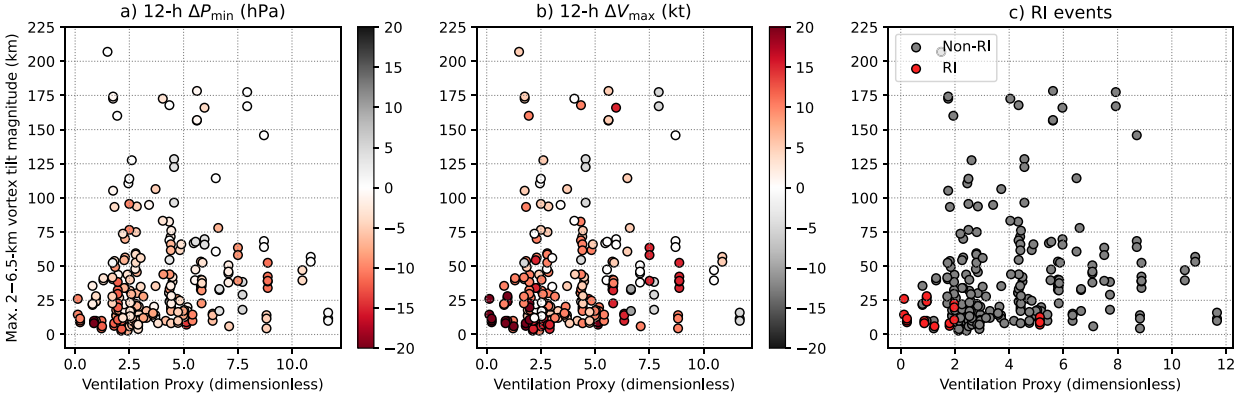

FIG. 7. (a) Scatterplot of the maximum 2–6.5-km vortex tilt magnitude (km) and ventilation proxy [VP; dimensionless; see Eq. (A1) for definition]. Each point represents a unique analysis, where the color of the marker corresponds to the future 12-h change in best track central pressure (ΔP_{min}). Here, only weak TCs were analyzed. Environmental data are derived from the synoptic time closest to the time of the TDR analysis. (b) As in (a), but the color of the marker corresponds to the future 12-h change in best track maximum sustained 10-m wind (ΔV_{max}). (c) As in (a) and (b), but cases are partitioned as either RI (red markers) or non-RI (gray markers) cases based on the future 12-h change in ΔV_{max}.

an aligned vortex, but if the environment is unfavorable, whether it be due to large shear, dry air, limited ocean heat content, or some other influence, the vortex may fail to intensify, or even weaken. The preference for TC intensification to occur when both vortex misalignment is relatively small and the environment is favorable is better illustrated in Fig. 7. Here, environmental favorability is defined by a new metric, referred to here as the ventilation proxy, which is similar to the "ventilation index" of Tang and Emanuel (2012), but uses existing SHIPS parameters. The ventilation proxy is defined as

$$\mathrm{VP} = \frac{\mathrm{SHDC}(100 - \mathrm{RHMD})}{\mathrm{MPI}}, \tag{1}$$

where SHDC is the deep-layer shear magnitude, RHMD is the 700–500-hPa mean relative humidity (%) averaged within a 200–800-km TC-centered annulus, and MPI is the environmental maximum potential intensity. Thus, smaller values of VP indicate a more favorable environment for TC intensification consistent with less ventilation of the TC warm core via low-entropy environmental air (e.g., Tang and Emanuel 2010, 2012). For the cases examined here, the ventilation proxy exhibited stronger correlations to future TC intensity change than its individual components, consistent with the findings of Lin et al. (2017). In this framework, RI is only observed to occur when vortex tilt is ≤30 km and VP values are approximately 5 or less (Fig. 7c). However, the majority of RI cases occur in environments with a ventilation proxy ≤ 2.0. In fact, of the 30 TDR analyses with a tilt magnitude ≤ 30 km and in an environment characterized by a VP ≤ 2.0, 17 were associated with subsequent RI, or approximately 57% of such cases. Alternatively, of the 205 remaining TDR analyses with either tilt magnitudes > 30 km or environments with a VP > 2.0, only 4 were associated with subsequent RI. Although a larger sample size would be preferred, the joint

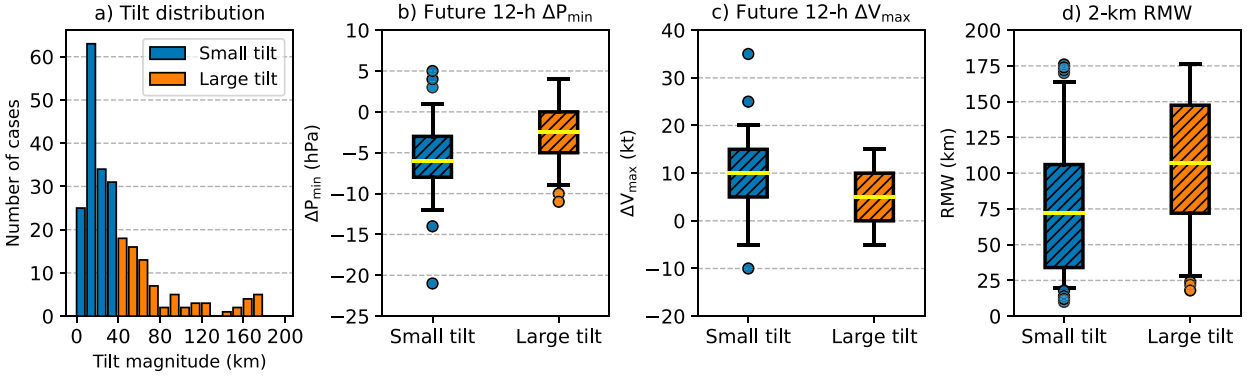

FIG. 8. (a) Histogram of tilt magnitude for the weak TCs examined in this study. Cases in the small-tilt and large-tilt groups are shaded in blue and orange, respectively. (b) Box-and-whisker plots of future 12-h change in the best track central pressure for small-tilt (blue) and large-tilt (orange) TCs. Here the shaded boxes span the 25th–75th percentiles, the yellow line indicates the median, and the whiskers span the 5th–95th percentiles. Outliers from these ranges are shown by the corresponding shaded circles. Hatched boxes indicate the differences in the distributions are statistically significant. (c) As in (b), but for the future 12-h change in best track maximum sustained 10-m wind. (d) As in (b), but for the distribution of the TDR-derived radius of maximum wind (RMW) at a height of 2.0 km.

TABLE 1. Mean TC intensity and environmental parameters for small- and large-tilt TCs. Bolded values indicate that differences in the distributions for each tilt group are statically significant at the 95% confidence level.

Tilt group	No. of TDR analyses	Intensity (kt)	Shear magnitude (m s^{-1})	700–500-hPa RH (%)	OHC (kJ cm^{-1})
Small tilt	153	**54.9**	**6.8**	60.5	44.4
Large tilt	82	**47.9**	**8.0**	58.9	45.6

parameter space shown in Fig. 7 is a promising framework to identify strong candidates to undergo RI.

c. *How is vortex tilt related to the TC precipitation structure?*

Thus far, we have shown TC intensification occurs preferentially for cases with small-tilt magnitudes in favorable environments. Furthermore, we have shown the magnitude of vortex tilt in weak TCs is a robust predictor of short-term intensity change (e.g., over 12–48 h), displaying a stronger correlation to TC intensity change than the environmental deep-layer wind shear magnitude. Next, we explore how the TC precipitation structure is associated with the magnitude of vortex tilt with the aim of understanding why TCs with small-tilt magnitudes intensify at greater rates than more misaligned vortices.

1) ESTABLISHING TWO TILT GROUPS: SMALL- AND LARGE-TILT TCS

To assess how the magnitude of vortex tilt impacts the TC precipitation structure, the remaining analyses will examine two groups of weak TCs based on the degree of vortex misalignment. Figure 8a shows a histogram of vortex tilt magnitude for all weak TCs and the partitioning of the two tilt groups. The first group, referred to as small-tilt TCs, are those where the tilt magnitude is <40 km. The second group, referred to as large-tilt TCs, are those where the tilt magnitude is ≥40 km. The threshold used to define the two groups is close to the mean tilt magnitude in weak TCs. Consistent with Fig. 3, small-tilt TCs intensify at greater rates than large-tilt TCs (Figs. 8b,c). The differences in TC intensity change for each group are statistically significant at the 99.9% confidence level.[10] Likewise, the distribution of the 2.0-km radius of maximum wind (RMW)[11] in small-tilt TCs is significantly smaller than that for large-tilt TCs (Fig. 8d), indicating small-tilt storms tend to have more compact inner cores than vortices with greater misalignment. The results in Fig. 8 are consistent with the idealized modeling results of Schecter (2022), who found smaller tilt magnitudes are associated with more compact inner cores and faster rates of TC development.

The number of cases, the mean TC intensities, and select environmental metadata for each tilt group are provided in Table 1. Small-tilt TCs tend to be slightly stronger than large-tilt TCs, which is consistent with the pattern shown in Fig. 2. Because small-tilt TCs are associated with more intense vortices with smaller RMWs (Fig. 8d) than large-tilt TCs, small-tilt vortices are generally characterized by larger Rossby numbers than large-tilt TCs, which has been shown to be a favorable characteristic for TC intensification (Miyamoto and Takemi 2015; X. Chen et al. 2018b; Miyamoto and Nolan 2018). Small-tilt TCs also experience statistically significant weaker shear than large-tilt TCs, although both tilt groups experience similar midtropospheric RH and OHC. Because of the limited observational sample size, the remaining analyses will not attempt to account for the intensity and shear differences between the tilt groups, but, rather, use the entire distribution of small- and large-tilt TCs and their respective environmental and intensity biases as observed in nature.

2) THE INFLUENCE OF VORTEX MISALIGNMENT ON THE HORIZONTAL TC PRECIPITATION STRUCTURE

To better understand how the degree of vortex misalignment is related to the TC precipitation structure, Fig. 9 shows tilt-relative, TDR-derived reflectivity at a height of 2.0 km. Figures 9a–c show the TC precipitation structure relative to the low-level (2.0-km) TC center (LLC). For reference, the average RMW for each group is also shown. Both small-tilt and large-tilt TCs are associated with a composite reflectivity maximum down-tilt of the TC center; however, large-tilt TCs are associated with a reflectivity maximum located at larger radii than small-tilt TCs. The radial location of peak reflectivities in the small-tilt composite is found inward of its average RMW (Fig. 9a), whereas in large-tilt TCs the location of strongest composite reflectivities is outward of its average RMW (Fig. 9b). Thus, the convective configuration in small-tilt TCs is more favorable for TC intensification, as heating focused inward of the RMW can facilitate the inward advection of angular momentum surfaces across the low-level RMW (e.g., Smith and Montgomery 2016).

Small-tilt TCs are also associated with greater reflectivities near and uptilt-left of the LLC than large-tilt TCs (Fig. 9c), indicating small-tilt storms feature a more symmetric precipitation structure. The more symmetric reflectivity and greater intensification rates in small-tilt TCs agrees with previous satellite-based studies that have linked more symmetric TC precipitation to greater TC intensification rates, including RI (Zagrodnik and Jiang 2014; Alvey et al. 2015; Tao and Jiang 2015; Fischer et al. 2018). Although these satellite-based studies could not resolve the TC tilt structure, the findings of the present study suggest it is plausible the more symmetric satellite-derived precipitation structures at RI onset may be related to relatively small vortex tilt magnitudes. This notion is supported by the fact that the mean TC intensity of "RI

[10] In this study, differences between distributions were determined to be statistically significant if a Wilcoxon rank-sum test yielded a p value < 0.05. In some cases, such as done here, higher confidence levels are specified.

[11] The RMW estimates in the present study contain an element of uncertainty due to gaps in observational coverage inherent to the TDR analyses. Subjective analysis of every TDR-derived wind field in the small-tilt and large-tilt groups provided confidence that systematic RMW differences between the two tilt groups exist.

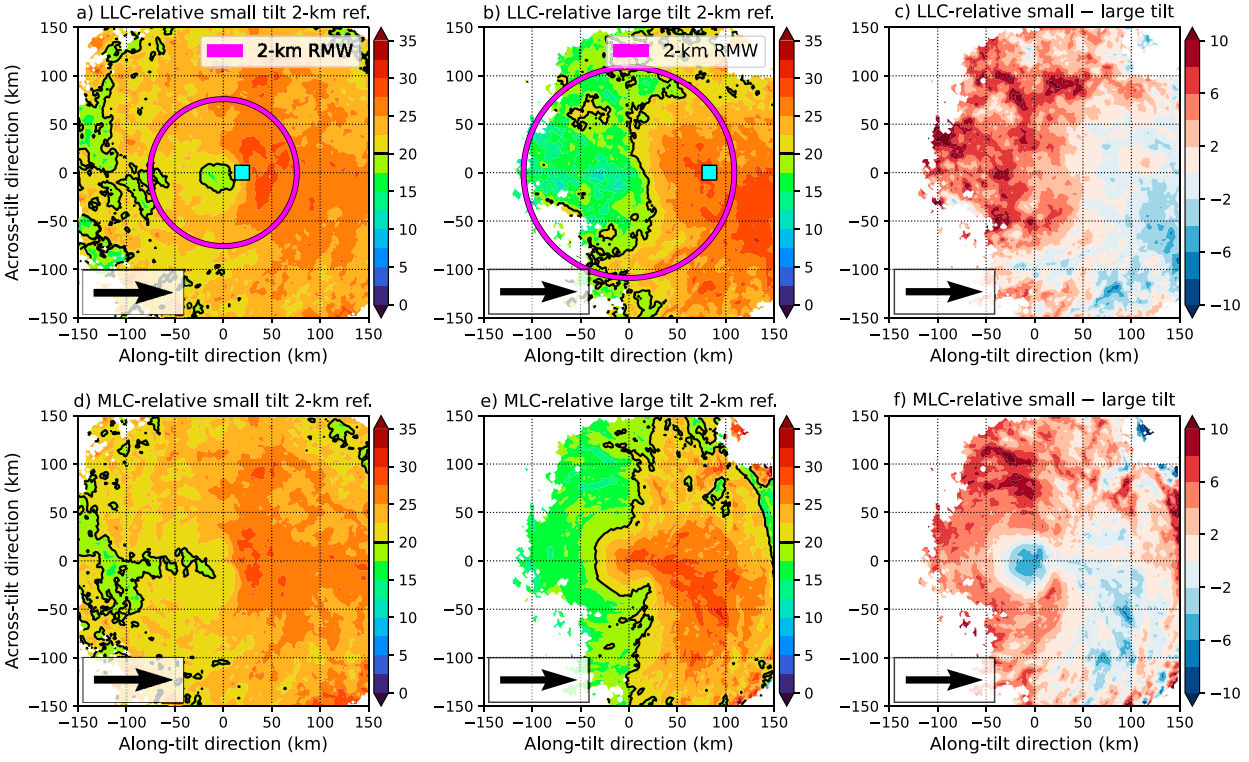

FIG. 9. (a) Storm-centered, tilt-relative, composite-mean reflectivity (shaded; dBZ) at a height of 2.0 km for all small-tilt TCs. Composites are constructed relative to the 2-km TC center location and shown within the innermost 150 km of the storm. A black contour highlights the 20-dBZ contour. The cyan square indicates the mean location of the MLC. The vortex tilt direction always points to the right side of the figure, as indicated by the black arrow. Values are only shown for locations with at least 10 data points. (b) As in (a), but for all large-tilt TCs. (c) As in (a), but for small-tilt minus large-tilt TCs. (d)–(f) As in (a)–(c), but composites are constructed relative to the MLC location. The MLC is defined as the location where vortex tilt is the largest for heights between 5 and 6.5 km.

onset" cases examined by Tao et al. (2017) was 54 kt, well within the range of the "weak" TCs examined here. Reanalysis output has also indicated a link between more aligned vortices, more symmetric precipitation structures, and greater TC intensification rates (Richardson et al. 2022); however, it is unclear whether the relatively coarse resolution of the reanalysis can accurately resolve the structure of vortex tilt for a given TC.

Nevertheless, the greater down-tilt displacement of enhanced reflectivities in large-tilt TCs shown in Figs. 9a–c suggests the location of the strongest convection in weak TCs may be closely tied to the location of the midlevel TC center (MLC[12]). To test this hypothesis, Figs. 9d–9f show the tilt-relative, 2.0-km reflectivity structure for composites constructed relative to the MLC location. A remarkably different reflectivity pattern is observed, especially for large-tilt TCs (Fig. 9e), which now feature curved bands of enhanced reflectivity that wrap cyclonically around the MLC location. In fact, large-tilt TCs are associated with greater reflectivities within the nearest 25–50 km of the MLC location than small-tilt TCs (Fig. 9f). The greater concentration of enhanced reflectivities near the MLC rather than the LLC in large-tilt storms is reminiscent of sheared TCs that have exposed lower-tropospheric circulation centers as seen in geostationary satellite imagery (cf. Fig. 9 in Nguyen et al. 2017) and agrees with previous observational case studies using airborne Doppler radar analyses (Nguyen et al. 2017; Rogers et al. 2020) and numerical modeling simulations (Tao and Zhang 2014; Rios-Berrios et al. 2018; Ryglicki et al. 2018; Alvey and Hazelton 2022; Schecter 2022). Idealized modeling simulations have shown mesoscale subsidence associated with the balanced response to a tilted TC vortex provides an unfavorable thermodynamic environment for convective activity near the LLC until vortex misalignment can be sufficiently reduced (Schecter 2022). The weaker reflectivities near the LLC in large-tilt TCs (Fig. 9b) are consistent with the notion of an unfavorable thermodynamic environment associated with mesoscale subsidence in the uptilt portion of the storm. It is also possible that the greater MLC displacement in large-tilt TCs facilitates the advection of dry environmental air near the LLC, weakening reflectivities there (e.g., Davis and Ahijevych 2012; Alland et al. 2021b; Fischer et al. 2023).

The radial structure of the reflectivity distribution at a height of 2.0 km in small-tilt and large-tilt TCs is illustrated in the form of contoured frequency by radius diagrams (CFRDs), shown in Fig. 10. Near the LLC, small-tilt TCs are associated

[12] The MLC is defined as the location where vortex tilt magnitude is the largest for heights between 5 and 6.5 km.

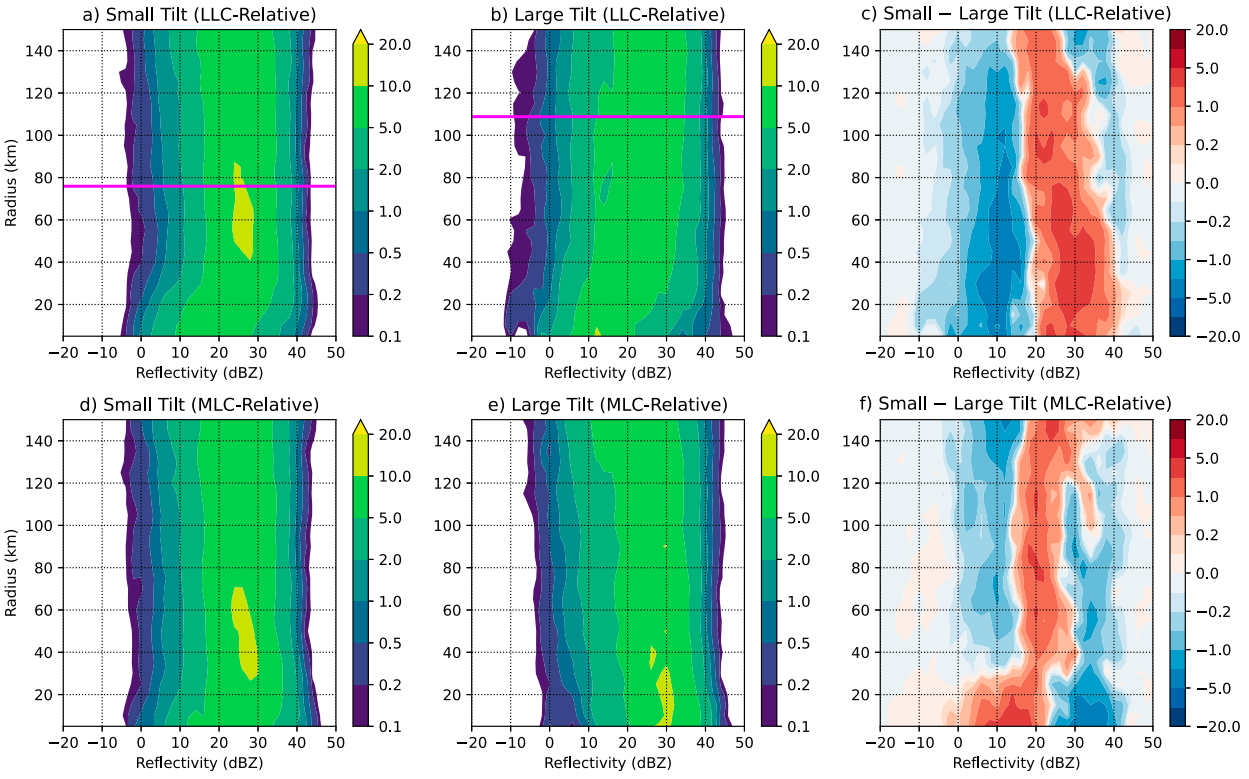

FIG. 10. (a) Contoured frequency by radius diagram of reflectivity (%) at a height of 2.0 km, relative to the low-level center (LLC) for all small-tilt TCs. Values are binned in increments of 2 dBZ and radii of 10 km. (b) As in (a), but for large-tilt TCs. (c) As in (a), but the difference between small-tilt minus large-tilt TCs. (d)–(f) As in (a)–(c), but for radius relative to the MLC location.

with a greater frequency of reflectivities > 20 dBZ than large-tilt storms throughout the innermost 50 km (Fig. 10c). Outward of 60–80 km, large-tilt TCs display a greater frequency of reflectivities > 35–40 dBZ, consistent with a greater frequency of more robust convective activity. Additionally, large-tilt TCs also have a greater frequency of relatively weak reflectivities (i.e., <20 dBZ) throughout the innermost 100 km of the LLC. If larger reflectivities are used as a proxy for greater diabatic heating (e.g., Guimond et al. 2011), Figs. 10a–c imply that small-tilt TCs are characterized by stronger diabatic heating near the LLC. In a framework relative to the MLC, large-tilt TCs are characterized by a greater frequency of reflectivities > 30 dBZ than small-tilt storms throughout the innermost 100 km (Figs. 10d–f). In both tilt groups, however, relatively large reflectivities (i.e., >35 dBZ) occur more frequently within 20 km of the MLC, as reflected by the contours that flare outward toward the right in Figs. 10d and 10e. Thus, the location of strongest reflectivities, and presumably strongest diabatic heating, is closely tied to the location of the MLC.

It is important to note that these TDR analyses can only provide a snapshot of the TC precipitation structure within a radius of approximately 50 km of the flight track due to the nature of the radar system. Thus, a given TDR analysis is likely to miss some regions of precipitation for an average-sized TC (Fischer et al. 2022). This aspect of the database raises some uncertainty over the robustness of the results shown in Figs. 9 and 10 due to the limited sample size at a given storm-relative grid point. To address this, Fig. 11 shows tilt-relative composites of IR brightness temperatures, relative to the location of the LLC, which are available for all small- and large-tilt TCs at all locations. The spatial pattern of IR brightness temperatures closely matches the 2.0-km TDR reflectivity shown in Figs. 9a–c, as small-tilt TCs are associated with more symmetric IR brightness temperatures, as well as a smaller radial displacement between the LLC and the strongest convection, than large-tilt TCs. Figure 11c shows small-tilt TCs feature statistically significant lower IR brightness temperatures throughout nearly the entirety of the uptilt-left quadrant and portions of the uptilt-right and downtilt-left quadrants. Conversely, large-tilt TCs have significantly lower IR brightness over a region approximately 100–200 km downtilt, and downtilt-right, of the LLC. The spatial patterns of IR brightness temperatures shown in Fig. 11 support the conclusions from Figs. 9 and 10 that small-tilt TCs are associated with significantly more symmetric TC convective structures, whereas convection in large-tilt TCs tends to be displaced downtilt, toward the MLC.

3) THE VERTICAL STRUCTURE AND MODE OF PRECIPITATION

The previous subsection demonstrated the degree of vortex misalignment is strongly related to the horizontal TC precipitation structure. To investigate how vortex misalignment is related to the vertical structure of TC precipitation, Figs. 12a–c

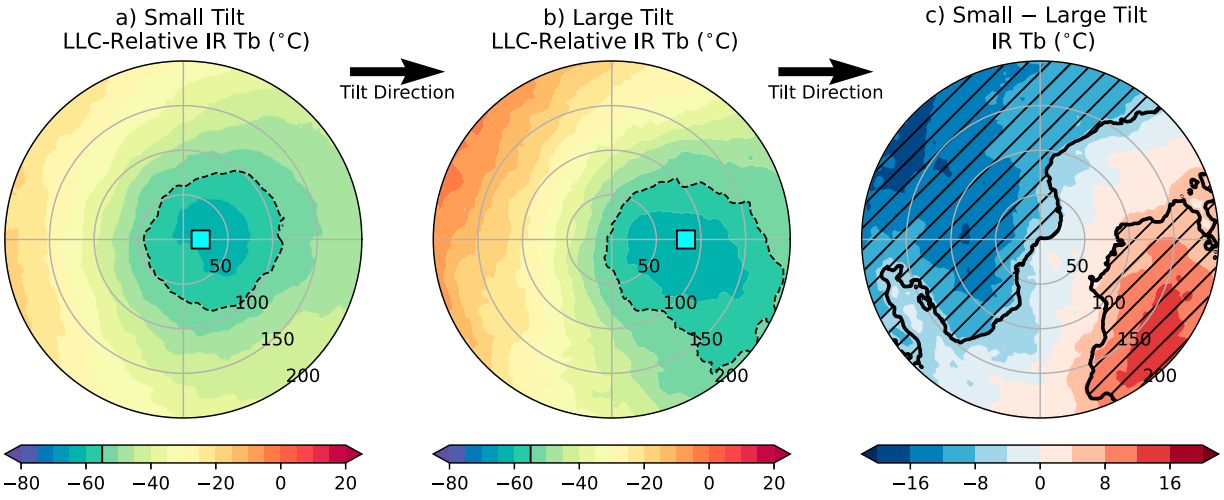

FIG. 11. (a) Storm-centered, tilt-relative, composite-mean IR brightness temperatures (shaded; °C) for all small-tilt TCs. Values are centered relative to the 2.0-km TC center location and shown within the innermost 200 km of the storm. Gray radial rings are shown in 50-km increments. The vortex tilt direction always points to the right side of the figure, as indicated by the black arrows. The dashed black contour indicates where composite IR brightness temperatures are <-55°C. The cyan square indicates the mean MLC location. (b) As in (a), but for all large-tilt TCs. (c) As in (a), but for small-tilt minus large-tilt TCs. Hatched regions indicate where differences are statistically significant at the 95% confidence level.

show contoured frequency by altitude diagrams (CFADs; Yuter and Houze 1995) of TDR-derived vertical velocity (V_W) within 50 km of the LLC for small-tilt and large-tilt TCs. The difference plot in Fig. 12c more readily shows how the distributions compare between the two groups. Below a height of approximately 5 km, small-tilt TCs display a greater frequency of relatively weak ascent (i.e., <1 m s^{-1}). Above 5 km, small-tilt TCs have a greater frequency of ascent for nearly all values < 5 m s^{-1}. At nearly all vertical levels, large-tilt TCs have a greater frequency of descent than small-tilt TCs, which is consistent with more widespread subsidence driven by the balanced response to a vertically misaligned vortex as well as the lack of strong reflectivities seen near the LLC in Figs. 9 and 10.

Near the MLC, large-tilt TCs are associated with a wider range of vertical velocities than small-tilt TCs (Figs. 12d–f), suggesting large-tilt TCs have a greater frequency of relatively vigorous convection. Alternatively, small-tilt TCs are associated with a greater frequency of weak vertical velocities throughout much of the troposphere.

CFADs of reflectivity (Fig. 13) provide further insight into the vertical structure of precipitation in each tilt group. Near the LLC, small-tilt TCs have a greater frequency of reflectivities > 20 dBZ below a height of 6–7 km, suggesting a greater frequency of either convective cores of shallow–moderate depth or stratiform precipitation (Figs. 13a–c). Interestingly, above a height of 8 km, large-tilt TCs have a greater frequency of relatively large reflectivities, implying a greater frequency of deep convection. Near the MLC, large-tilt TCs consistently have a greater frequency of the relatively large reflectivities, again supporting a greater frequency of deep convection.

To better understand how the mode of precipitation differs between the two tilt groups, an objective TC precipitation partitioning algorithm was employed. The partitioning algorithm is described in detail in appendix C. To summarize here, radar reflectivity at each analysis grid point is classified as one of five types: 1) weak echo, 2) stratiform, 3) shallow convection, 4) moderate convection, or 5) deep convection. The distinction between weak echo, stratiform, and convection is based on the horizontal reflectivity pattern at a height of 2.0 km, whereas the type of convection (e.g., shallow, moderate, or deep) is based on the vertical structure of reflectivity at that grid point.

Using the objective precipitation partitioning, the distributions of each precipitation mode in small-tilt and large-tilt TCs were inspected (Fig. 14). For regions within 50 km of the LLC (Fig. 14a), small-tilt TCs are associated with significantly less weak echo regions and significantly more stratiform precipitation than large-tilt TCs. Alvey et al. (2020) used an ensemble of simulations of the same storm to show cases with smaller vortex tilt magnitudes experience a greater azimuthal advection of hydrometeors and humidification from stratiform precipitation. The greater prevalence of stratiform precipitation in small-tilt TCs in the current database is consistent with this finding. Figure 14a also shows that small-tilt TCs are associated with a significantly greater frequency of moderate convection near the LLC, which agrees with the reflectivity CFADs shown in Figs. 13a–c. Previous observational case studies have highlighted the importance of a greater frequency of convection of moderate depth, which is associated with a vertical mass flux profile that favors vortex stretching in the lower-troposphere (Raymond et al. 2014; Rogers et al. 2020; Alvey et al. 2022; Stone et al. 2023). While these studies focused on processes leading up to vortex alignment, it is unclear from the present study whether the greater frequency of moderate convection near the LLC in small-tilt TCs is the cause or result of a nearly aligned vortex. Regardless, increases in the frequency of stratiform precipitation and moderate convection have been shown to be favorable for greater rates of TC intensification (Tao and Jiang 2015; Tao et al. 2017; Alvey et al. 2022; Stone et al. 2023).

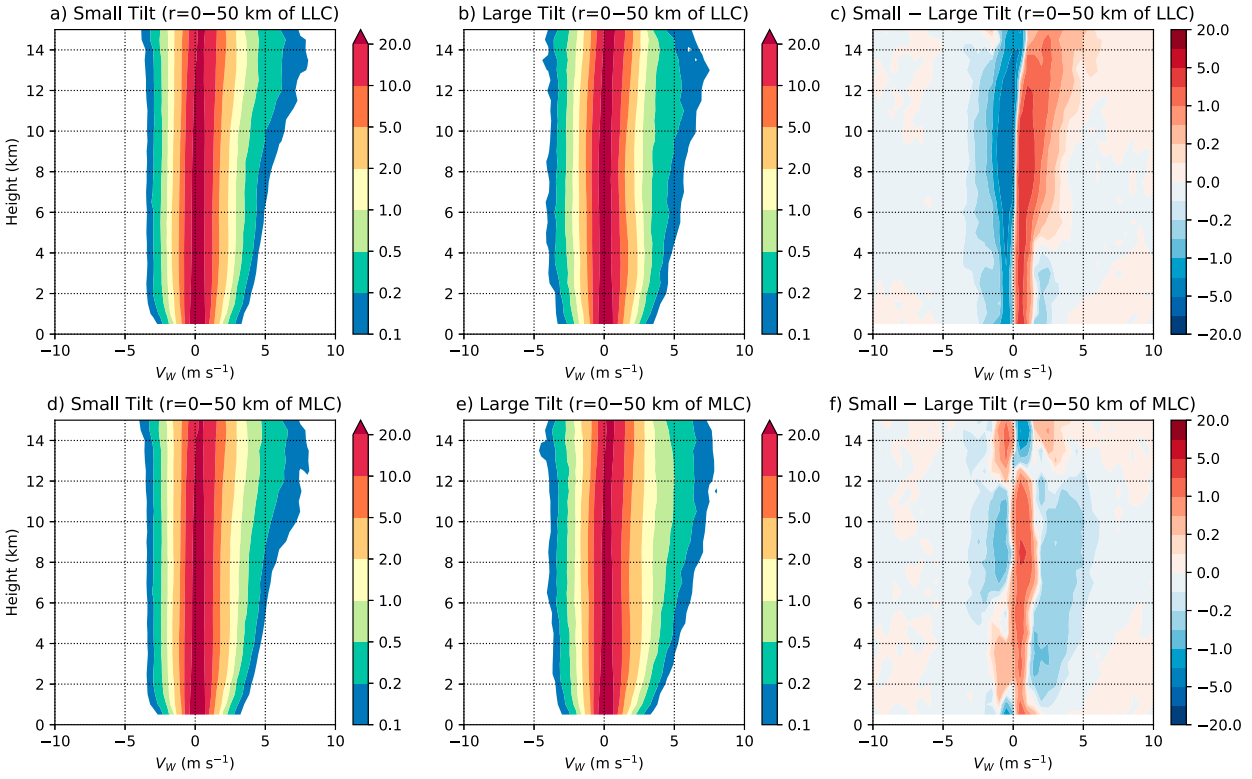

FIG. 12. (a) Contoured frequency by altitude diagram (CFAD) of vertical velocity (V_w; %) using all analysis grid points within 50 km of the 2-km TC center for small-tilt TCs. Values are binned in increments of 0.5 m s^{-1}. (b) As in (a), but for large-tilt TCs. (c) As in (a), but the difference between small-tilt minus large-tilt TCs. (d)–(f) As in (a)–(c), but for all analysis grid points within 50 km of the MLC location.

If the distribution of each precipitation mode is computed within 50 km of the MLC (Fig. 14b) instead of near the LLC, the differences in stratiform and moderate convection regions between small- and large-tilt TCs essentially vanish. This change results from an increase in the frequency of stratiform precipitation and moderate convection, and a decrease in weak echo regions, compared to regions near the LLC in large-tilt TCs. The predominance of stratiform precipitation near the MLC that is common to both tilt groups suggest this mode of precipitation—and its relatively top-heavy mass flux profile and associated midlevel vorticity generation (e.g., Gjorgjievska and Raymond 2014; Fuchs-Stone et al. 2020)—is important for maintaining and influencing the location of the MLC, consistent with previous modeling studies (Tao and Zhang 2014; Rios-Berrios et al. 2018; Alvey and Hazelton 2022).

Curiously, small-tilt TCs are associated with significantly more frequent weak echo regions and shallow convection than large-tilt TCs near the MLC. Although no statistically significant differences in the frequency of deep convection were found between small-tilt and large-tilt TCs (Fig. 14), the tilt-relative reflectivity composites (Fig. 9), the CFRDs of reflectivity (Fig. 10), as well as the V_W and reflectivity CFADs (Figs. 12 and 13) all indicate more misaligned vortices favor more vigorous and deeper convection, especially in the vicinity of the MLC, than small-tilt TCs. While the lack of widespread thermodynamic observations prevented computations of buoyancy, the preference for more vigorous convective activity near the MLC in large-tilt storms agrees with previous studies that have indicated the down-tilt cold anomaly associated with a balanced vortex can provide enhanced buoyancy for ascending parcels in the lower troposphere (Rios-Berrios et al. 2018; Ryglicki et al. 2018; Boehm and Bell 2021; Schecter 2022). Regardless of the driver of the convection, the results of this study have demonstrated the TC precipitation structure in weak TCs is strongly connected to the degree of vortex misalignment as well as the position of the midtropospheric TC center.

4. Conclusions

Although multiple previous studies have found the transition from a vertically misaligned vortex toward an aligned state to be favorable for TC intensification, the role of vortex alignment in the TC intensification process has been ambiguous, with some studies finding vortex alignment occurs following the beginning of an intensification event rather than acting as the trigger of TC intensification (e.g., Chen and Gopalakrishnan 2015; X. Chen et al. 2018b). In this study, we sought to elucidate the relationships between vortex misalignment, TC precipitation structure, and future intensity change in nature. To achieve this goal, the present study used a recently introduced airborne Doppler radar database, referred to as TC-RADAR, which contains over 1100 unique analyses

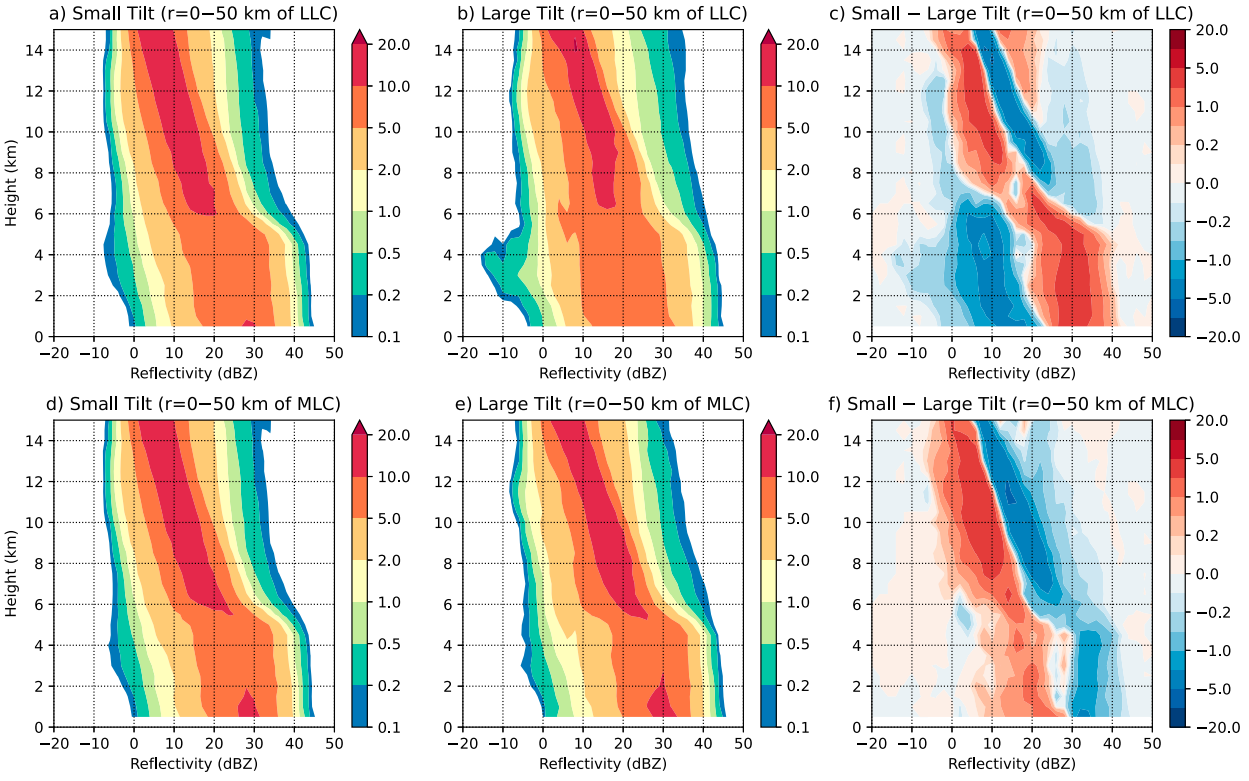

FIG. 13. (a) CFAD of reflectivity (%) using all analysis grid points within 50 km of the 2-km TC center for small-tilt TCs. Values are binned in increments of 2 dBZ. (b) As in (a), but for large-tilt TCs. (c) As in (a), but the difference between small-tilt minus large-tilt TCs. (d)–(f) As in (a)–(c), but for all analysis grid points within 50 km of the MLC location.

for TCs across a wide range of intensities. A novel TC center-finding method was implemented that allowed for estimates of vortex tilt from individual TDR analyses where sufficient data coverage existed. It is our understanding this is the first study of its kind, as previous observational studies that have examined vortex misalignment have been limited to either case studies or analyses of storms of hurricane intensity. The present study was made possible, in large part, by recent efforts to more frequently observe early-stage TCs as part of NOAA's hurricane field program (Zawislak et al. 2022). Key findings from the current analysis are summarized below:

- In weak TCs (defined here as TCs with intensities $\leq$ 65 kt), short-term TC intensity change (e.g., over a 12-h period) is more closely related to the magnitude of vortex tilt than the deep-layer shear magnitude at the beginning of the intensity change episode.
- Although most weak TCs tend to intensify regardless of the degree of vortex misalignment, TC intensification occurs at greater rates for storms with smaller tilt magnitudes.
- In mature hurricanes, large vortex tilt magnitudes are not observed and the relationship between vortex tilt and TC intensity change is weaker.
- For the cases examined in this study, RI occurs preferentially in storms with nearly aligned vortices.
- TC intensity change is ultimately governed by multiscale interactions. Some cases with small vortex tilt magnitudes were not observed to intensify presumably due to the influences of unfavorable environmental conditions. The TCs that intensified the most rapidly had both small vortex tilt magnitudes and a favorable environment.
- In weak TCs, the TC precipitation structure is closely linked to the degree of vortex misalignment and location of the midtropospheric TC center. TCs with large-tilt magnitudes tended to have the most vigorous convection, especially near the midtropospheric TC center.
- Near the lower-tropospheric TC center of weak TCs, small-tilt TCs have a greater frequency of ascent throughout much of the troposphere. A precipitation partitioning algorithm revealed the more frequent ascent in small-tilt TCs was associated with a greater frequency of stratiform precipitation and convection of moderate depth as well as fewer weak-echo regions.
- Tilt-relative composites indicated small-tilt TCs feature more symmetric reflectivities and stronger reflectivities near the lower-tropospheric TC center than large-tilt storms. The strongest composite reflectivities in small-tilt TCs are found inward of the average RMW location, whereas the opposite pattern is found in large-tilt TCs.
- We hypothesize TCs with smaller tilt magnitudes intensify at greater rates than large-tilt TCs due to a greater areal extent of diabatic heating near the lower-tropospheric TC center and inward of the RMW. Thus, small-tilt TCs are associated with a convective configuration that is favorable

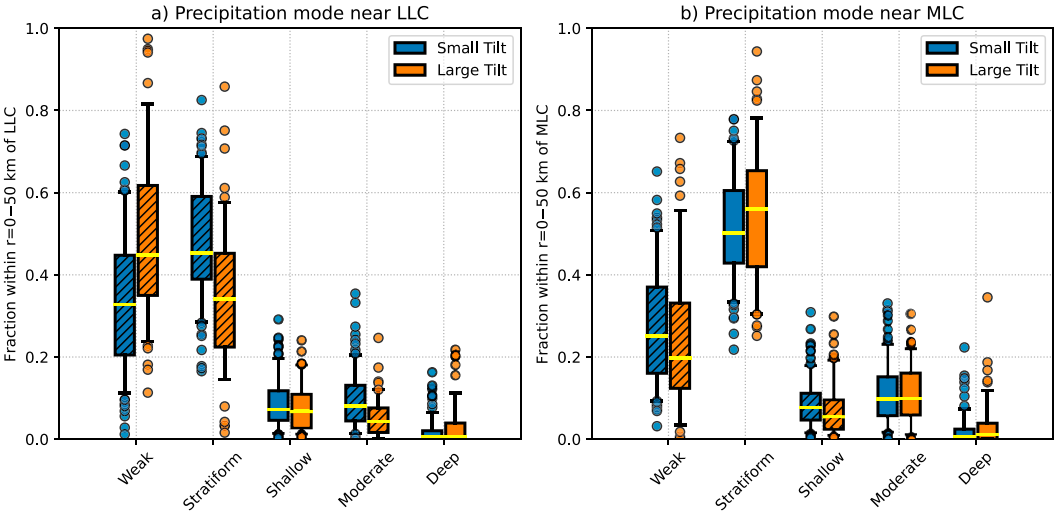

FIG. 14. (a) Box-and-whisker plots of the frequency of five precipitation modes (weak echo, stratiform, shallow convection, moderate convection, and deep convection) for all TDR analysis grid points within 50 km of the low-level (2-km) TC center (LLC) location. Distributions of the precipitation mode are shown for TCs in the small-tilt (blue) and large-tilt (orange) groups. Here the shaded boxes span the 25th–75th percentiles, the yellow line indicates the median, and the whiskers span the 5th–95th percentiles. Outliers from these ranges are shown by the corresponding shaded circles. Black hatching indicates the distribution of the precipitation type in each tilt group is statistically significantly different at the 95% confidence level. (b) As in (a), but for TDR analysis grid points within 50 km of the midlevel TC center (MLC). The MLC is defined as the location where vortex tilt is the largest for heights between 5 and 6.5 km.

for the inward advection of angular momentum surfaces across the location of the RMW in the boundary layer, which is required for TC intensification (e.g., Smith and Montgomery 2016).

These results highlight the utility of airborne Doppler radar observations in not only assessing TC structure, but using this information to assess the likelihood of TC intensification and RI. Because TDR analyses are transmitted in real time for display in the Advanced Weather Interactive Processing System (AWIPS-II), which is used by NOAA's National Weather Service centers such as the National Hurricane Center, information about the TC vortex tilt structure can be incorporated into the operational forecasting process (Zawislak et al. 2022). The real-time transmission of TDR analyses is complemented by the operational assimilation of TDR observations into the Hurricane Weather Research and Forecasting (HWRF) system, which has been shown to result in improvements in the model's forecast skill (Tong et al. 2018; Christophersen et al. 2022; Zawislak et al. 2022). TDR observations will also be assimilated into the next generation of high-resolution hurricane model guidance, the Hurricane Analysis and Forecasts System (HAFS; Hazelton et al. 2021; Alvey and Hazelton 2022; Zawislak et al. 2022; Hazelton et al. 2023).

The findings of the present study open the door for intriguing follow-up research opportunities. For example, would the addition of observational estimates of vortex tilt improve operational statistical models of TC intensity? Considering an aligned vortex appears to be an important structural requirement for RI, it is possible estimates of vortex tilt could be used to aid RI forecasts, which are the events responsible for the largest TC intensity forecast errors (Trabing and Bell 2020). Other important questions that remain to be answered include: why do some TCs with relatively large-tilt magnitudes intensify fairly quickly, but not others? Because instantaneous estimates of vortex tilt are used in the present study to quantify relationships to intensity change, it is quite possible some TCs experience a reduction in tilt shortly after the time of analysis (e.g., <6 h), which would provide a more favorable configuration for TC intensification. One example of a pathway where tilt can be rapidly reduced is vortex reformation, where a new lower-tropospheric TC center forms closer to the midtropospheric TC center through the impacts of strong diabatic heating and the associated bottom-heavy vertical mass flux profiles (Nguyen and Molinari 2015; X. Chen et al. 2018a; Rogers et al. 2020; Alvey et al. 2022; Nam et al. 2023; Rivera-Torres et al. 2023; Stone et al. 2023). Considering the present study revealed convective activity in misaligned, weak TCs occurs preferentially near the location of the midtropospheric TC center, vortex reformation events may help explain some of the variability in the relationship between TC intensity change and the degree of vortex misalignment observed here. Indeed, idealized modeling studies, such as Schecter and Menelaou (2020), have found time-averaged values of tilt magnitude correspond more closely to TC intensity change than instantaneous snapshots. In the present study, however, sampling rate limitations rendered the calculation of temporally averaged tilt infeasible. In a similar vein, the present study did not explore how misaligned vortices transition toward a more upright configuration (i.e., transition from the large-tilt to small-tilt regime); however, ongoing

work by the current authors is using TC-RADAR to gain insight into the physical processes responsible for vortex alignment in nature.

Acknowledgments. This project benefited from helpful conversations with Dr. Xiaomin Chen (University of Alabama in Huntsville) and Dr. Sim Aberson (NOAA/OAR/Atlantic Oceanographic and Meteorological Laboratory) as well as internal reviews provided by Drs. George Alvey and Andrew Hazelton (University of Miami and NOAA/OAR/Atlantic Oceanographic and Meteorological Laboratory). This work was supported by the Office of Naval Research Award N00014-20-1-2057 and National Science Foundation Award 2241605.

Data availability statement. The TC-RADAR data files, the bias-corrected reflectivities, and the storm-centered infrared brightness temperatures used in the present study are available at https://doi.org/10.5281/zenodo.10014658. The latest version, as well as select archived versions, of TC-RADAR can be found at https://www.aoml.noaa.gov/ftp/pub/hrd/data/radar/level3/. The SHIPS developmental data are located at https://rammb.cira.colostate.edu/research/tropical_cyclones/ships/developmental_data.asp. The MergIR database is available at https://disc.gsfc.nasa.gov/datasets/GPM_MERGIR_1/summary.

APPENDIX A

Revisions to the Weighted Circulation Maximization (WCM) Center-Finding Method

This study uses a modified version of the WCM center-finding technique introduced in Fischer et al. (2022) and was revised to yield more accurate TC center estimates from TDR swath analyses. The essence of the center-finding method is unchanged: a TC center is identified as the analysis grid point that produces the best match with an idealized vortex of purely cyclonic flow as determined by a cost function. The main changes implemented in the current version of the WCM center-finding technique can be summarized as follows: changing the components of the cost function, applying the cost function to a larger spatial domain, searching a larger domain for the TC center, and implementing additional data coverage constraints.

As before, the cost function is computed for a series of potential TC center candidates (the determination of potential TC center candidates is detailed later). The cost function used to determine the similarity between the idealized vortex of cyclonic flow and the given TDR analysis used in the current study is

$$\epsilon = \frac{1}{n}\sum_{i=1}^{n} |\delta_i \alpha_i|, \tag{A1}$$

where ϵ is the average weighted deviation (i.e., error) between the observed storm-relative horizontal wind and the idealized, cyclonic vortex for all grid points with available TDR observations within the domain of interest, n is the number of grid points with available data within the domain, i is the index of a given grid point, δ is a weighting function for the error and α is the angle of the deviation between the observed storm-relative horizontal wind direction and the idealized, cyclonic vortex centered on the potential TC center location to be tested. Although Eq. (A1) is identical to Eq. (A1) in Fischer et al. (2022), in the present study we define δ and α as

$$\delta = \frac{G}{\text{avg}(G)}\sqrt{|V_H| + 1}, \tag{A2}$$

$$G = \max(e^{-r^2/2R^2}, 10^{-6}), \tag{A3}$$

$$\alpha = \theta_{\text{obs}} - \theta_{\text{ideal}}, \tag{A4}$$

where G is a Gaussian-weighted distance function, with a minimum bound of 10^{-6}, r is the radius of the given grid point from the potential TC center, "avg" indicates the average of all points with observations, and R is a scaling radius used in the distance weighting function G and helps to determine the spatial scale of the vortex for which a center is being determined. Here, we use a value of 50 km for R, which is larger than the value of 25 km used in Fischer et al. (2022). This change was found to improve the consistency and reliability of the center estimates. $|V_H|$ is the magnitude of the storm-relative, horizontal wind at the given grid point (units of m s^{-1}). The terms θ_{obs} and θ_{ideal} are the mathematical angles, in radians, of the observed flow field and the idealized, cyclonic vortex, respectively. The TC center is ultimately determined to be the analysis grid point that yields the smallest value of ϵ.

To save computational time, Eq. (A1) was computed iteratively using potential TC centers within a subset of the original analysis domain. During the first iteration, potential TC centers are selected incrementally, where only one out of every five grid points are considered in both the meridional and zonal directions within a 100 km × 100 km region, centered on the location of maximum area-averaged relative vorticity, also within a 100 km × 100 km region. The purpose of this coarse search through the analysis domain is to identify the approximate location where the circulation is most pronounced. For the next step, all nearby grid points on the native 2-km horizontal grid spacing within a 20 km × 20 km domain, centered on the grid point that yielded the lowest value of ϵ from the previous iteration, were treated as potential TC centers, with ϵ calculated at each location. Then using the grid point that yielded the lowest value of ϵ from the previous iteration, ϵ was again computed within a new 20 km × 20-km centered-domain. This process was repeated until the same potential TC center location yielded the lowest value of ϵ over consecutive iterations and that grid point was determined to be the final TC center. For each iteration, the selection of a potential TC center was not dependent upon whether a wind observation is present at the grid point. Thus, a TC center can be identified at a grid point without any wind observations provided at least 15% of analysis grid points within radii of 50 and 100 km have TDR observations. Here we compute Eq. (A1) using all analysis grid points within 150 km of a potential TC center, which is larger than the 100-km radius used in Fischer et al. (2022).

To summarize, compared to the original WCM method introduced in Fischer et al. (2022), the key changes made to the revised WCM center-finding method were the following:

- Modify the calculation of δ [Eq. (A2)] to no longer have arbitrarily determined coefficients and, instead, multiply the Gaussian-weighted distance term by the square root of the wind speed plus the integer 1
- Use a value of R equal to 50 km, instead of R equal to 25 km
- Decrease the minimum bound of G to a smaller value of 10^{-6} as Eq. (A1) is now computed for all grid points within 150 km of the TC center (compared to all points within 100 km before)
- Consider larger search domains when iterating to identify the optimal center location
- Use a first-guess center estimate based on an area-averaged vorticity maximum
- Implement two coverage criteria, where at least 15% of all grid points within radii of 50 and 100 km must have TDR coverage (previous only 15% of all grid points within 100 km of the TC center needed to have data)

It is important to note that these center estimates contain an element of uncertainty. While this uncertainty is difficult to quantify, it is certainly a function of TDR data coverage. Employing more strict data coverage constraints would increase confidence in the center estimates, but would also limit the number of cases to examine, especially for cases with asymmetric precipitation structures and limited scatterers. Although some sensitivity tests were performed to examine how changing the distance scaling radius R influences the TC center estimate (not shown), future work would benefit from more thoroughly quantifying these impacts. Ensembles of TC center estimates using different values of R may provide a useful method of approximating TC center, and vortex tilt, uncertainty.

APPENDIX B

Reflectivity Bias-Correction Procedure

As noted in Wadler et al. (2023), the distribution of TDR-derived radar reflectivities can differ from aircraft-to-aircraft or from year to year. To reduce the impact of these observational biases in the results of the present study, a bias-correction technique was implemented following the methods of Wadler et al. (2023), except for a key distinction. Here, reflectivities were bias-corrected using a probability-matching technique based on two reference distributions: one reference distribution for years before a solid-state TDR system was used (years prior to 2017; Fig. B1a) and another for years after the solid-state TDR system was introduced (beginning in 2017; Fig. B1b). This distinction was implemented based on the solid-state TDR system's increased sensitivity to relatively weak reflectivities compared to previous TDR systems (Fischer et al. 2022). This increased sensitivity of the solid-state TDR can be seen in the percentile

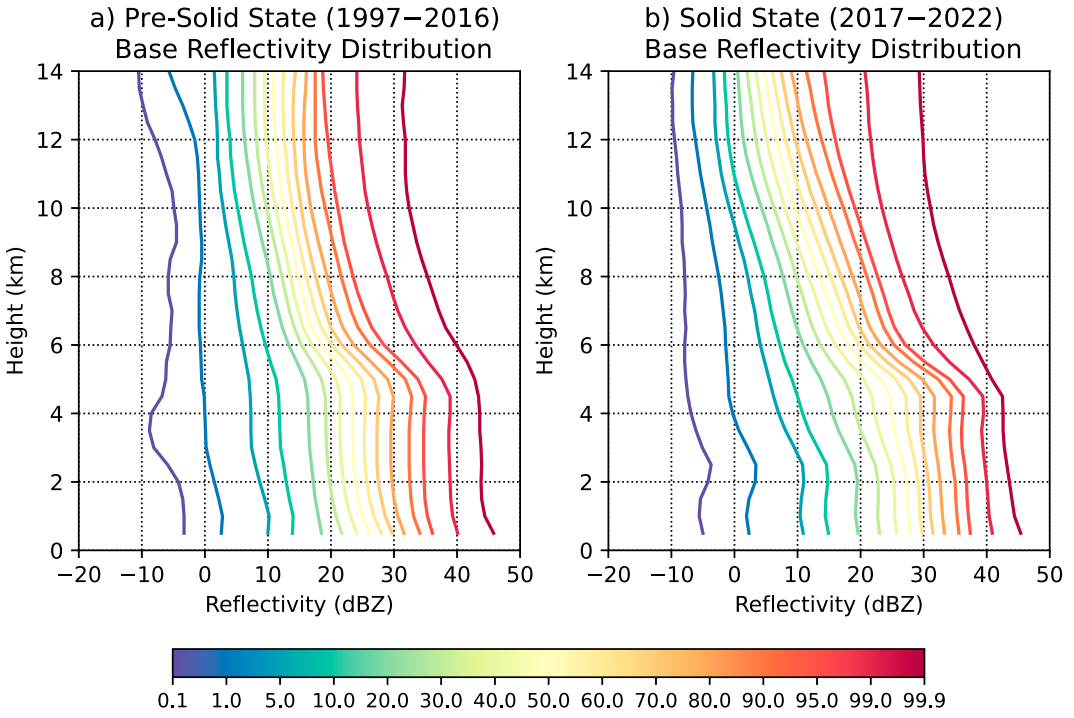

FIG. B1. (a) Distribution of different percentiles of the reference reflectivity (dBZ) distribution used in the reflectivity bias correction process, as a function of height (km). Here, only the pre-solid-state TDR era is considered (1997–2016). Each percentile corresponds to the values shown on the color bar. (b) As in (a), but for the solid-state TDR era (2017–22).

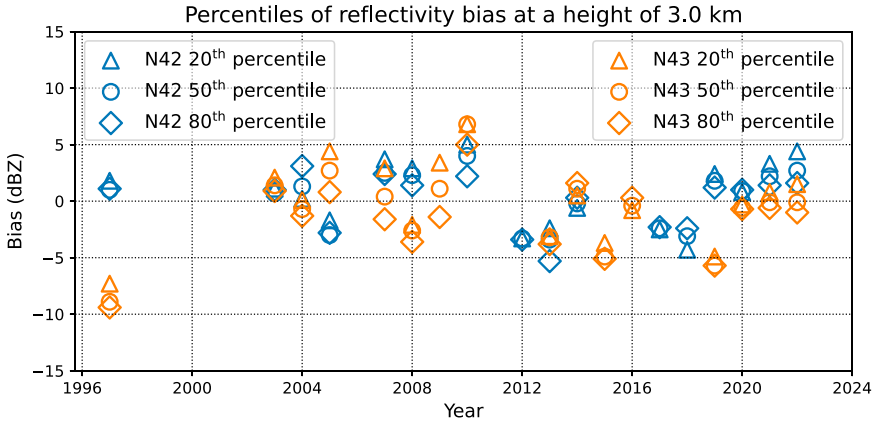

FIG. B2. Time series of the annual reflectivity bias-correction values (dBZ) applied to each aircraft (N42 in blue and N43 in orange) for select percentiles (20th, 50th, and 80th percentiles shown by the triangle, circle, and diamond-shaped markers, respectively) at an analysis height of 3.0 km. It should be noted that in certain years, TC-RADAR contains analyses from only one aircraft (e.g., 2009, 2012, and 2015–18), thus, only data from the single aircraft is shown.

contours at heights above 8 km in Fig. B1b, which bend toward the left with height (indicative of the identification of a greater frequency of weaker reflectivities) compared to the corresponding contours in pre-solid-state TDR era (Fig. B1a), which are more vertically oriented.

The premise of this reflectivity-bias correction technique is the assumption that using these two reference distributions will smooth most interseason biases and serve as two "truth" distributions. To implement the reflectivity bias-correction, for a given season, we identified flights where the two P3 aircraft (N42 and N43) observed the same TC within 12 h of each other. This temporal constraint assumes the storms have relatively similar distributions of reflectivity and that the external forcing on the storms, the intensity of the storms, and the convective structure of the storms are not changing significantly over a 12-h period. If two or more pairs of flights satisfied this temporal constraint in the same year, the observed radar reflectivity distributions for only the near-coincident flights were compared to the corresponding reference reflectivity distribution shown in Fig. B1. Otherwise, the distribution from all overwater flights from each aircraft within a given season was considered. A probability matching technique was then used to determine the relevant bias correction to apply to the observed reflectivity, which is discussed in more detail in Wadler et al. (2023). The bias-corrections used in the present study, as a function of the year and aircraft, are shown in Fig. B2. Although we only show the 3.0-km analysis height in Fig. B2, other analysis heights were found to follow a similar pattern.

APPENDIX C

Objective Precipitation Partitioning Method

To classify the mode of precipitation, this study employed an objective TC precipitation partitioning algorithm. This partitioning algorithm is similar to that used by Rogers et al. (2020) and Wadler et al. (2023). In the present study, precipitation is classified as one of five types based on the spatial pattern of radar reflectivity: 1) Weak echo, 2) stratiform, 3) shallow convection, 4) moderate convection, or 5) deep convection. A TDR analysis grid point was classified as weak echo if the reflectivity at a height of 2.0 km was $<$20 dBZ. If the 2-km reflectivity was $\geq$35 dBZ or satisfied a "peakedness" criteria (e.g., Steiner et al. 1995; Didlake and Houze 2009), the grid point was classified as convective. The depth of the convective type (e.g., shallow, moderate, or deep) was determined using the height of the 20-dBZ reflectivity contour. A convective grid point was classified as moderate or deep convection if a vertically continuous region of reflectivity $\geq$20 dBZ reached a height of at least 6 or 10 km, respectively. Otherwise, the convective grid point was classified as shallow convection. If the grid point did not meet the weak-echo or convective criteria, it was classified as stratiform.

An example of the precipitation partitioning scheme is shown in Fig. C1 for the case of Tropical Storm Earl (2010). A region of moderate and deep convection was identified near the location of the 7.0-km TC center (Fig. C1b). A west–east vertical cross section through this convective region compares the vertical profile of reflectivity to the objective partitioning (Fig. C1c).

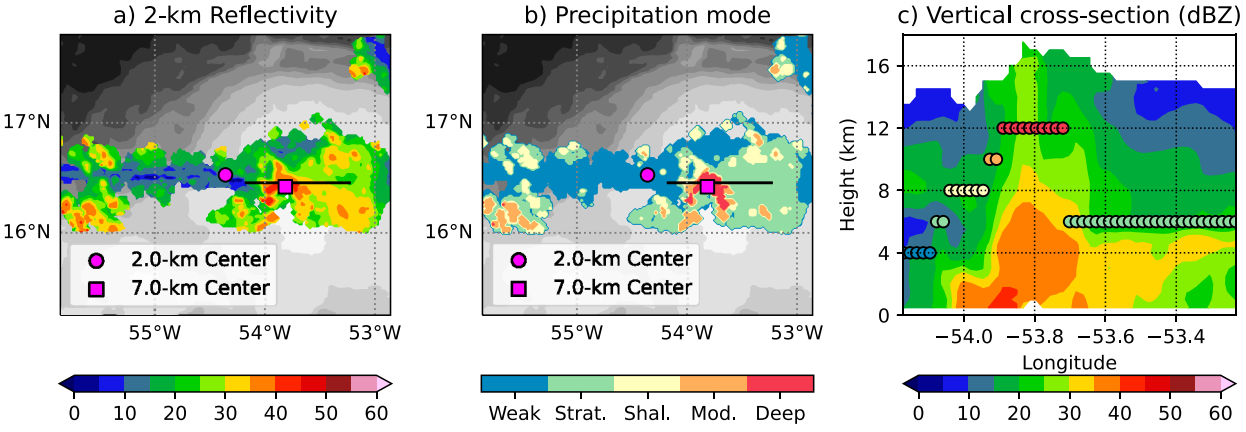

FIG. C1. (a) The 2-km reflectivity (color shading; dBZ) and IR brightness temperatures (grayscale shading; °C) for Tropical Storm Earl at 2251 UTC 28 Aug 2010. The objectively identified TC center at heights of 2 and 7 km are shown by the magenta circle and square markers, respectively. (b) As in (a), but here the precipitation mode is shown by the color shading. (c) A west–east-oriented vertical cross section of reflectivity (shaded; dBZ) taken along the black line shown in (a) and (b). The colored circle markers correspond to the precipitation mode using the same shading shown in (b).

For example, the shallow convective core near 54.0°W was classified as shallow convection, whereas eastward of this location, approaching 53.8°W, the height of the convection increases, and deep convection is identified. Farther eastward, a band of stratiform precipitation is identified, which exhibits an elevated maximum of reflectivity near the height of the melting level at 4.5 km, a hallmark of stratiform precipitation (Hence and Houze 2012; Didlake and Houze 2013).

REFERENCES

Alland, J. J., B. H. Tang, K. L. Corbosiero, and G. H. Bryan, 2021a: Combined effects of midlevel dry air and vertical wind shear on tropical cyclone development. Part I: Downdraft ventilation. *J. Atmos. Sci.*, **78**, 763–782, https://doi.org/10.1175/JAS-D-20-0054.1.

——, ——, ——, and ——, 2021b: Combined effects of midlevel dry air and vertical wind shear on tropical cyclone development. Part II: Radial ventilation. *J. Atmos. Sci.*, **78**, 783–796, https://doi.org/10.1175/JAS-D-20-0055.1.

Alvey, G. R., III, and A. Hazelton, 2022: How do weak, misaligned tropical cyclones evolve toward alignment? A multicase study using the hurricane analysis and forecast system. *J. Geophys. Res. Atmos.*, **127**, e2022JD037268, https://doi.org/10.1029/2022JD037268.

——, J. Zawislak, and E. Zipser, 2015: Precipitation properties observed during tropical cyclone intensity change. *Mon. Wea. Rev.*, **143**, 4476–4492, https://doi.org/10.1175/MWR-D-15-0065.1.

——, E. Zipser, and J. Zawislak, 2020: How does Hurricane Edouard (2014) evolve toward symmetry before rapid intensification? A high-resolution ensemble study. *J. Atmos. Sci.*, **77**, 1329–1351, https://doi.org/10.1175/JAS-D-18-0355.1.

——, M. Fischer, P. Reasor, J. Zawislak, and R. Rogers, 2022: Observed processes underlying the favorable vortex repositioning early in the development of Hurricane Dorian (2019). *Mon. Wea. Rev.*, **150**, 193–213, https://doi.org/10.1175/MWR-D-21-0069.1.

Boehm, A. M., and M. M. Bell, 2021: Retrieved thermodynamic structure of Hurricane Rita (2005) from airborne multi–Doppler radar data. *J. Atmos. Sci.*, **78**, 1583–1605, https://doi.org/10.1175/JAS-D-20-0195.1.

Cangialosi, J. P., E. Blake, M. DeMaria, A. Penny, A. Latto, E. Rappaport, and V. Tallapragada, 2020: Recent progress in tropical cyclone intensity forecasting at the National Hurricane Center. *Wea. Forecasting*, **35**, 1913–1922, https://doi.org/10.1175/WAF-D-20-0059.1.

Carrasco, C. A., C. W. Landsea, and Y.-L. Lin, 2014: The influence of tropical cyclone size on its intensification. *Wea. Forecasting*, **29**, 582–590, https://doi.org/10.1175/WAF-D-13-00092.1.

Chen, B.-F., C. A. Davis, and Y.-H. Kuo, 2018: Effects of low-level flow orientation and vertical shear on the structure and intensity of tropical cyclones. *Mon. Wea. Rev.*, **146**, 2447–2467, https://doi.org/10.1175/MWR-D-17-0379.1.

Chen, H., and S. G. Gopalakrishnan, 2015: A study on the asymmetric rapid intensification of Hurricane Earl (2010) using the HWRF system. *J. Atmos. Sci.*, **72**, 531–550, https://doi.org/10.1175/JAS-D-14-0097.1.

Chen, X., Y. Wang, J. Fang, and M. Xue, 2018a: A numerical study on rapid intensification of Typhoon Vicente (2012) in the South China Sea. Part II: Roles of inner-core processes. *J. Atmos. Sci.*, **75**, 235–255, https://doi.org/10.1175/JAS-D-17-0129.1.

——, M. Xue, and J. Fang, 2018b: Rapid intensification of Typhoon Mujigae (2015) under different sea surface temperatures: Structural changes leading to rapid intensification. *J. Atmos. Sci.*, **75**, 4313–4335, https://doi.org/10.1175/JAS-D-18-0017.1.

——, J.-F. Gu, J. A. Zhang, F. D. Marks, R. F. Rogers, and J. J. Cione, 2021: Boundary layer recovery and precipitation symmetrization preceding rapid intensification of tropical cyclones under shear. *J. Atmos. Sci.*, **78**, 1523–1544, https://doi.org/10.1175/JAS-D-20-0252.1.

Christophersen, H., J. Sippel, A. Aksoy, and N. L. Baker, 2022: Recent advancements for tropical cyclone data assimilation. *Ann. N.Y. Acad. Sci.*, **1517**, 25–43, https://doi.org/10.1111/nyas.14873.

Cram, T. A., J. Persing, M. T. Montgomery, and S. A. Braun, 2007: A Lagrangian trajectory view on transport and mixing processes between the eye, eyewall, and environment using a

high-resolution simulation of Hurricane Bonnie (1998). *J. Atmos. Sci.*, **64**, 1835–1856, https://doi.org/10.1175/JAS3921.1.

Davis, C. A., and D. A. Ahijevych, 2012: Mesoscale structural evolution of three tropical weather systems observed during PREDICT. *J. Atmos. Sci.*, **69**, 1284–1305, https://doi.org/10.1175/JAS-D-11-0225.1.

DeMaria, M., 1996: The effect of vertical shear on tropical cyclone intensity change. *J. Atmos. Sci.*, **53**, 2076–2088, https://doi.org/10.1175/1520-0469(1996)053<2076:TEOVSO>2.0.CO;2.

——, and J. Kaplan, 1994: A Statistical Hurricane Intensity Prediction Scheme (SHIPS) for the Atlantic basin. *Wea. Forecasting*, **9**, 209–220, https://doi.org/10.1175/1520-0434(1994)009<0209:ASHIPS>2.0.CO;2.

——, and ——, 1999: An updated Statistical Hurricane Intensity Prediction Scheme (SHIPS) for the Atlantic and eastern North Pacific basins. *Wea. Forecasting*, **14**, 326–337, https://doi.org/10.1175/1520-0434(1999)014<0326:AUSHIP>2.0.CO;2.

——, M. Mainelli, L. K. Shay, J. A. Knaff, and J. Kaplan, 2005: Further improvements to the Statistical Hurricane Intensity Prediction Scheme (SHIPS). *Wea. Forecasting*, **20**, 531–543, https://doi.org/10.1175/WAF862.1.

——, C. R. Sampson, J. A. Knaff, and K. D. Musgrave, 2014: Is tropical cyclone intensity guidance improving? *Bull. Amer. Meteor. Soc.*, **95**, 387–398, https://doi.org/10.1175/BAMS-D-12-00240.1.

DesRosiers, A. J., M. M. Bell, and T.-Y. Cha, 2022: Vertical vortex development in Hurricane Michael (2018) during rapid intensification. *Mon. Wea. Rev.*, **150**, 99–114, https://doi.org/10.1175/MWR-D-21-0098.1.

——, ——, P. J. Klotzbach, M. S. Fischer, and P. D. Reasor, 2023: Observed relationships between tropical cyclone vortex height, intensity, and intensification rate. *Geophys. Res. Lett.*, **50**, e2022GL101877, https://doi.org/10.1029/2022GL101877.

Didlake, A. C., Jr., and R. A. Houze Jr., 2009: Convective-scale downdrafts in the principal rainband of Hurricane Katrina (2005). *Mon. Wea. Rev.*, **137**, 3269–3293, https://doi.org/10.1175/2009MWR2827.1.

——, and ——, 2013: Dynamics of the stratiform sector of a tropical cyclone rainband. *J. Atmos. Sci.*, **70**, 1891–1911, https://doi.org/10.1175/JAS-D-12-0245.1.

Emanuel, K., C. DesAutels, C. Holloway, and R. Korty, 2004: Environmental control of tropical cyclone intensity. *J. Atmos. Sci.*, **61**, 843–858, https://doi.org/10.1175/1520-0469(2004)061<0843:ECOTCI>2.0.CO;2.

Finocchio, P. M., and S. J. Majumdar, 2017: A statistical perspective on wind profiles and vertical wind shear in tropical cyclone environments of the Northern Hemisphere. *Mon. Wea. Rev.*, **145**, 361–378, https://doi.org/10.1175/MWR-D-16-0221.1.

——, and R. Rios-Berrios, 2021: The intensity- and size-dependent response of tropical cyclones to increasing vertical wind shear. *J. Atmos. Sci.*, **78**, 3673–3690, https://doi.org/10.1175/JAS-D-21-0126.1.

——, S. J. Majumdar, D. S. Nolan, and M. Iskandarani, 2016: Idealized tropical cyclone responses to the height and depth of environmental vertical wind shear. *Mon. Wea. Rev.*, **144**, 2155–2175, https://doi.org/10.1175/MWR-D-15-0320.1.

Fischer, M. S., B. H. Tang, K. L. Corbosiero, and C. M. Rozoff, 2018: Normalized convective characteristics of tropical cyclone rapid intensification events in the North Atlantic and eastern North Pacific. *Mon. Wea. Rev.*, **146**, 1133–1155, https://doi.org/10.1175/MWR-D-17-0239.1.

——, ——, and ——, 2019: A climatological analysis of tropical cyclone rapid intensification in environments of upper-tropospheric troughs. *Mon. Wea. Rev.*, **147**, 3693–3719, https://doi.org/10.1175/MWR-D-19-0013.1.

——, P. D. Reasor, R. F. Rogers, and J. F. Gamache, 2022: An analysis of tropical cyclone vortex and convective characteristics in relation to storm intensity using a novel airborne Doppler radar database. *Mon. Wea. Rev.*, **150**, 2255–2278, https://doi.org/10.1175/MWR-D-21-0223.1.

——, ——, B. H. Tang, K. L. Corbosiero, R. D. Torn, and X. Chen, 2023: A tale of two vortex evolutions: Using a high-resolution ensemble to assess the impacts of ventilation on a tropical cyclone rapid intensification event. *Mon. Wea. Rev.*, **151**, 297–320, https://doi.org/10.1175/MWR-D-22-0037.1.

Fuchs-Stone, Ž., D. J. Raymond, and S. Sentić, 2020: OTREC2019: Convection over the East Pacific and southwest Caribbean. *Geophys. Res. Lett.*, **47**, e2020GL087564, https://doi.org/10.1029/2020GL087564.

Gjorgjievska, S., and D. J. Raymond, 2014: Interaction between dynamics and thermodynamics during tropical cyclogenesis. *Atmos. Chem. Phys.*, **14**, 3065–3082, https://doi.org/10.5194/acp-14-3065-2014.

Guimond, S. R., G. M. Heymsfield, and F. J. Turk, 2010: Multiscale observations of Hurricane Dennis (2005): The effects of hot towers on rapid intensification. *J. Atmos. Sci.*, **67**, 633–654, https://doi.org/10.1175/2009JAS3119.1.

——, M. A. Bourassa, and P. D. Reasor, 2011: A latent heat retrieval and its effects on the intensity and structure change of Hurricane Guillermo (1997). Part I: The algorithm and observations. *J. Atmos. Sci.*, **68**, 1549–1567, https://doi.org/10.1175/2011JAS3700.1.

——, G. M. Heymsfield, P. D. Reasor, and A. C. Didlake Jr., 2016: The rapid intensification of Hurricane Karl (2010): New remote sensing observations of convective bursts from the global Hawk platform. *J. Atmos. Sci.*, **73**, 3617–3639, https://doi.org/10.1175/JAS-D-16-0026.1.

Hazelton, A., L. Harris, and S.-J. Lin, 2018: Evaluation of tropical cyclone structure forecasts in a high-resolution version of the multiscale GFDL fvGFS model. *Wea. Forecasting*, **33**, 419–442, https://doi.org/10.1175/WAF-D-17-0140.1.

——, and Coauthors, 2021: 2019 Atlantic hurricane forecasts from the global-nested hurricane analysis and forecast system: Composite statistics and key events. *Wea. Forecasting*, **36**, 519–538, https://doi.org/10.1175/WAF-D-20-0044.1.

——, G. J. Alaka Jr., M. S. Fischer, R. Torn, and S. Gopalakrishnan, 2023: Factors influencing the track of Hurricane Dorian (2019) in the west Atlantic: Analysis of a HAFS ensemble. *Mon. Wea. Rev.*, **151**, 175–192, https://doi.org/10.1175/MWR-D-22-0112.1.

Hence, D. A., and R. A. Houze Jr., 2012: Vertical structure of tropical cyclone rainbands as seen by the TRMM Precipitation Radar. *J. Atmos. Sci.*, **69**, 2644–2661, https://doi.org/10.1175/JAS-D-11-0323.1.

Huntley, J. E., and J. W. Diercks, 1981: The occurrence of vertical tilt in tropical cyclones. *Mon. Wea. Rev.*, **109**, 1689–1700, https://doi.org/10.1175/1520-0493(1981)109<1689:TOOVTI>2.0.CO;2.

Janowiak, J., B. Joyce, and P. Xie, 2017: NCEP/CPC L3 half hourly 4km global (60S–60N) merged IR V1 (GPM_MERGIR). Goddard Earth Sciences Data and Information Services Center (GES DISC), accessed 17 June 2022, https://doi.org/10.5067/P4HZB9N27EKU.

Jones, S. C., 1995: The evolution of vortices in vertical shear. I: Initially barotropic vortices. *Quart. J. Roy. Meteor. Soc.*, **121**, 821–851, https://doi.org/10.1002/qj.49712152406.

——, 2000: The evolution of vortices in vertical shear. III: Baroclinic vortices. *Quart. J. Roy. Meteor. Soc.*, **126**, 3161–3185, https://doi.org/10.1002/qj.49712657009.

Kaplan, J., M. DeMaria, and J. A. Knaff, 2010: A revised tropical cyclone rapid intensification index for the Atlantic and eastern North Pacific basins. *Wea. Forecasting*, **25**, 220–241, https://doi.org/10.1175/2009WAF2222280.1.

——, and Coauthors, 2015: Evaluating environmental impacts on tropical cyclone rapid intensification predictability utilizing statistical models. *Wea. Forecasting*, **30**, 1374–1396, https://doi.org/10.1175/WAF-D-15-0032.1.

Knaff, J. A., C. R. Sampson, and M. DeMaria, 2005: An operational statistical typhoon intensity prediction scheme for the western North Pacific. *Wea. Forecasting*, **20**, 688–699, https://doi.org/10.1175/WAF863.1.

Leighton, H., S. Gopalakrishnan, J. A. Zhang, R. F. Rogers, Z. Zhang, and V. Tallapragada, 2018: Azimuthal distribution of deep convection, environmental factors, and tropical cyclone rapid intensification: A perspective from HWRF ensemble forecasts of Hurricane Edouard (2014). *J. Atmos. Sci.*, **75**, 275–295, https://doi.org/10.1175/JAS-D-17-0171.1.

Lin, N., R. Jing, Y. Wang, E. Yonekura, J. Fan, and L. Xue, 2017: A statistical investigation of the dependence of tropical cyclone intensity change on the surrounding environment. *Mon. Wea. Rev.*, **145**, 2813–2831, https://doi.org/10.1175/MWR-D-16-0368.1.

Martinez, J., M. M. Bell, J. L. Vigh, and R. F. Rogers, 2017: Examining tropical cyclone structure and intensification with the FLIGHT+ dataset from 1999 to 2012. *Mon. Wea. Rev.*, **145**, 4401–4421, https://doi.org/10.1175/MWR-D-17-0011.1.

Miyamoto, Y., and T. Takemi, 2015: A triggering mechanism for rapid intensification of tropical cyclones. *J. Atmos. Sci.*, **72**, 2666–2681, https://doi.org/10.1175/JAS-D-14-0193.1.

——, and D. S. Nolan, 2018: Structural changes preceding rapid intensification in tropical cyclones as shown in a large ensemble of idealized simulations. *J. Atmos. Sci.*, **75**, 555–569, https://doi.org/10.1175/JAS-D-17-0177.1.

Morss, R. E., J. Vickery, H. Lazrus, J. Demuth, and A. Bostrom, 2022: Improving tropical cyclone forecast communication by understanding NWS partners' decision timelines and forecast information needs. *Wea. Climate Soc.*, **14**, 783–800, https://doi.org/10.1175/WCAS-D-21-0170.1.

Nam, C. C., M. M. Bell, and D. Tao, 2023: Bifurcation points for tropical cyclone genesis and intensification in sheared and dry environments. *J. Atmos. Sci.*, **80**, 2239–2259, https://doi.org/10.1175/JAS-D-22-0100.1.

Nguyen, L. T., and J. Molinari, 2015: Simulation of the downshear reformation of a tropical cyclone. *J. Atmos. Sci.*, **72**, 4529–4551, https://doi.org/10.1175/JAS-D-15-0036.1.

——, R. F. Rogers, and P. D. Reasor, 2017: Thermodynamic and kinematic influences on precipitation symmetry in sheared tropical cyclones: Bertha and Cristobal (2014). *Mon. Wea. Rev.*, **145**, 4423–4446, https://doi.org/10.1175/MWR-D-17-0073.1.

Nolan, D. S., and L. D. Grasso, 2003: Nonhydrostatic, three-dimensional perturbations to balanced, hurricane-like vortices. Part II: Symmetric response and nonlinear simulations. *J. Atmos. Sci.*, **60**, 2717–2745, https://doi.org/10.1175/1520-0469(2003)060<2717:NTPTBH>2.0.CO;2.

——, and M. G. McGauley, 2012: Tropical cyclogenesis in wind shear: Climatological relationships and physical processes. *Cyclones: Formation, Triggers and Control*, K. Oouchi and H. Fudeyasu, Eds., Nova Science Publishers, 1–35.

——, Y. Moon, and D. P. Stern, 2007: Tropical cyclone intensification from asymmetric convection: Energetics and efficiency. *J. Atmos. Sci.*, **64**, 3377–3405, https://doi.org/10.1175/JAS3988.1.

Onderlinde, M. J., and D. S. Nolan, 2017: The tropical cyclone response to changing wind shear using the method of time-varying point-downscaling. *J. Adv. Model. Earth Syst.*, **9**, 908–931, https://doi.org/10.1002/2016MS000796.

Raymond, D. J., S. Gjorgjievska, S. Sessions, and Z. Fuchs, 2014: Tropical cyclogenesis and mid-level vorticity. *Aust. Meteor. Oceanogr. J.*, **64**, 11–25, https://doi.org/10.22499/2.6401.003.

Reasor, P. D., and M. D. Eastin, 2012: Rapidly intensifying Hurricane Guillermo (1997). Part II: Resilience in shear. *Mon. Wea. Rev.*, **140**, 425–444, https://doi.org/10.1175/MWR-D-11-00080.1.

——, M. T. Montgomery, and L. D. Grasso, 2004: A new look at the problem of tropical cyclones in vertical shear flow: Vortex resiliency. *J. Atmos. Sci.*, **61**, 3–22, https://doi.org/10.1175/1520-0469(2004)061<0003:ANLATP>2.0.CO;2.

——, ——, and L. F. Bosart, 2005: Mesoscale observations of the genesis of Hurricane Dolly (1996). *J. Atmos. Sci.*, **62**, 3151–3171, https://doi.org/10.1175/JAS3540.1.

——, R. Rogers, and S. Lorsolo, 2013: Environmental flow impacts on tropical cyclone structure diagnosed from airborne Doppler radar composites. *Mon. Wea. Rev.*, **141**, 2949–2969, https://doi.org/10.1175/MWR-D-12-00334.1.

Richardson, J. C., R. D. Torn, and B. H. Tang, 2022: An analog comparison between rapidly and slowly intensifying tropical cyclones. *Mon. Wea. Rev.*, **150**, 2139–2156, https://doi.org/10.1175/MWR-D-21-0260.1.

Riemer, M., M. T. Montgomery, and M. E. Nicholls, 2010: A new paradigm for intensity modification of tropical cyclones: Thermodynamic impact of vertical wind shear on the inflow layer. *Atmos. Chem. Phys.*, **10**, 3163–3188, https://doi.org/10.5194/acp-10-3163-2010.

Rios-Berrios, R., 2020: Impacts of radiation and cold pools on the intensity and vortex tilt of weak tropical cyclones interacting with vertical wind shear. *J. Atmos. Sci.*, **77**, 669–689, https://doi.org/10.1175/JAS-D-19-0159.1.

——, and R. D. Torn, 2017: Climatological analysis of tropical cyclone intensity changes under moderate vertical wind shear. *Mon. Wea. Rev.*, **145**, 1717–1738, https://doi.org/10.1175/MWR-D-16-0350.1.

——, ——, and C. A. Davis, 2016: An ensemble approach to investigate tropical cyclone intensification in sheared environments. Part II: Ophelia (2011). *J. Atmos. Sci.*, **73**, 1555–1575, https://doi.org/10.1175/JAS-D-15-0245.1.

——, C. A. Davis, and R. D. Torn, 2018: A hypothesis for the intensification of tropical cyclones under moderate vertical wind shear. *J. Atmos. Sci.*, **75**, 4149–4173, https://doi.org/10.1175/JAS-D-18-0070.1.

Rivera-Torres, N. G., K. L. Corbosiero, and B. H. Tang, 2023: Factors associated with the downshear reformation of tropical cyclones. *Mon. Wea. Rev.*, **151**, 2717–2737, https://doi.org/10.1175/MWR-D-22-0251.1.

Rogers, R. F., P. Reasor, and S. Lorsolo, 2013: Airborne Doppler observations of the inner-core structural differences between intensifying and steady-state tropical cyclones. *Mon. Wea. Rev.*, **141**, 2970–2991, https://doi.org/10.1175/MWR-D-12-00357.1.

——, P. D. Reasor, and J. A. Zhang, 2015: Multiscale structure and evolution of Hurricane Earl (2010) during rapid intensification. *Mon. Wea. Rev.*, **143**, 536–562, https://doi.org/10.1175/MWR-D-14-00175.1.

——, J. A. Zhang, J. Zawislak, H. Jiang, G. R. Alvey III, E. J. Zipser, and S. N. Stevenson, 2016: Observations of the

structure and evolution of Hurricane Edouard (2014) during intensity change. Part II: Kinematic structure and the distribution of deep convection. *Mon. Wea. Rev.*, **144**, 3355–3376, https://doi.org/10.1175/MWR-D-16-0017.1.

——, P. D. Reasor, J. A. Zawislak, and L. T. Nguyen, 2020: Precipitation processes and vortex alignment during the intensification of a weak tropical cyclone in moderate vertical shear. *Mon. Wea. Rev.*, **148**, 1899–1929, https://doi.org/10.1175/MWR-D-19-0315.1.

Ryglicki, D. R., J. D. Doyle, Y. Jin, D. Hodyss, and J. H. Cossuth, 2018: The unexpected rapid intensification of tropical cyclones in moderate vertical wind shear. Part II: Vortex tilt. *Mon. Wea. Rev.*, **146**, 3801–3825, https://doi.org/10.1175/MWR-D-18-0021.1.

Schecter, D. A., 2022: Intensification of tilted tropical cyclones over relatively cool and warm oceans in idealized numerical simulations. *J. Atmos. Sci.*, **79**, 485–512, https://doi.org/10.1175/JAS-D-21-0051.1.

——, and K. Menelaou, 2020: Development of a misaligned tropical cyclone. *J. Atmos. Sci.*, **77**, 79–111, https://doi.org/10.1175/JAS-D-19-0074.1.

Shi, D., and G. Chen, 2021: The implication of outflow structure for the rapid intensification of tropical cyclones under vertical wind shear. *Mon. Wea. Rev.*, **149**, 4107–4127, https://doi.org/10.1175/MWR-D-21-0141.1.

Sippel, J. A., J. W. Nielsen-Gammon, and S. E. Allen, 2006: The multiple-vortex nature of tropical cyclogenesis. *Mon. Wea. Rev.*, **134**, 1796–1814, https://doi.org/10.1175/MWR3165.1.

Smith, R. K., and M. T. Montgomery, 2016: The efficiency of diabatic heating and tropical cyclone intensification. *Quart. J. Roy. Meteor. Soc.*, **142**, 2081–2086, https://doi.org/10.1002/qj.2804.

Steiner, M., R. A. Houze Jr., and S. E. Yuter, 1995: Climatological characterization of three-dimensional storm structure from operational radar and rain gauge data. *J. Appl. Meteor.*, **34**, 1978–2007, https://doi.org/10.1175/1520-0450(1995)034<1978:CCOTDS>2.0.CO;2.

Stevenson, S. N., K. L. Corbosiero, and J. Molinari, 2014: The convective evolution and rapid intensification of Hurricane Earl (2010). *Mon. Wea. Rev.*, **142**, 4364–4380, https://doi.org/10.1175/MWR-D-14-00078.1.

——, ——, M. DeMaria, and J. L. Vigh, 2018: A 10-year survey of tropical cyclone inner-core lightning bursts and their relationship to intensity change. *Wea. Forecasting*, **33**, 23–36, https://doi.org/10.1175/WAF-D-17-0096.1.

Stone, Z., G. Alvey III, J. P. Dunion, M. S. Fischer, D. J. Raymond, R. F. Rogers, S. Sentić, and J. Zawislak, 2023: Thermodynamic contribution to vortex alignment and rapid intensification of Hurricane Sally (2020). *Mon. Wea. Rev.*, **151**, 931–951, https://doi.org/10.1175/MWR-D-22-0201.1.

Tang, B., and K. Emanuel, 2010: Midlevel ventilation's constraint on tropical cyclone intensity. *J. Atmos. Sci.*, **67**, 1817–1830, https://doi.org/10.1175/2010JAS3318.1.

——, and ——, 2012: A ventilation index for tropical cyclones. *Bull. Amer. Meteor. Soc.*, **93**, 1901–1912, https://doi.org/10.1175/BAMS-D-11-00165.1.

Tao, C., and H. Jiang, 2015: Distributions of shallow to very deep precipitation— Convection in rapidly intensifying tropical cyclones. *J. Climate*, **28**, 8791–8824, https://doi.org/10.1175/JCLI-D-14-00448.1.

——, ——, and J. Zawislak, 2017: The relative importance of stratiform and convective rainfall in rapidly intensifying tropical cyclones. *Mon. Wea. Rev.*, **145**, 795–809, https://doi.org/10.1175/MWR-D-16-0316.1.

Tao, D., and F. Zhang, 2014: Effect of environmental shear, sea-surface temperature, and ambient moisture on the formation and predictability of tropical cyclones: An ensemble-mean perspective. *J. Adv. Model. Earth Syst.*, **6**, 384–404, https://doi.org/10.1002/2014MS000314.

——, and ——, 2019: Evolution of dynamic and thermodynamic structures before and during rapid intensification of tropical cyclones: Sensitivity to vertical wind shear. *Mon. Wea. Rev.*, **147**, 1171–1191, https://doi.org/10.1175/MWR-D-18-0173.1.

——, M. Bell, R. Rotunno, and P. J. van Leeuwen, 2020: Why do the maximum intensities in modeled tropical cyclones vary under the same environmental conditions? *Geophys. Res. Lett.*, **47**, e2019GL085980, https://doi.org/10.1029/2019GL085980.

Tong, M., and Coauthors, 2018: Impact of assimilating aircraft reconnaissance observations on tropical cyclone initialization and prediction using operational HWRF and GSI ensemble–variational hybrid data assimilation. *Mon. Wea. Rev.*, **146**, 4155–4177, https://doi.org/10.1175/MWR-D-17-0380.1.

Trabing, B. C., and M. M. Bell, 2020: Understanding error distributions of hurricane intensity forecasts during rapid intensity changes. *Wea. Forecasting*, **35**, 2219–2234, https://doi.org/10.1175/WAF-D-19-0253.1.

Wadler, J. B., R. F. Rogers, and P. D. Reasor, 2018: The relationship between spatial variations in the structure of convective bursts and tropical cyclone intensification as determined by airborne Doppler radar. *Mon. Wea. Rev.*, **146**, 761–780, https://doi.org/10.1175/MWR-D-17-0213.1.

——, D. S. Nolan, J. A. Zhang, and L. K. Shay, 2021: Thermodynamic characteristics of downdrafts in tropical cyclones as seen in idealized simulations of different intensities. *J. Atmos. Sci.*, **78**, 3503–3524, https://doi.org/10.1175/JAS-D-21-0006.1.

——, J. J. Cione, R. F. Rogers, and M. S. Fischer, 2023: On the distribution of convective and stratiform precipitation in tropical cyclones from airborne Doppler radar and its relationship to intensity change and environmental wind shear direction. *Mon. Wea. Rev.*, **151**, 3209–3233, https://doi.org/10.1175/MWR-D-23-0048.1.

Yuter, S. E., and R. A. Houze Jr., 1995: Three-dimensional kinematic and microphysical evolution of Florida cumulonimbus. Part II: Frequency distributions of vertical velocity, reflectivity, and differential reflectivity. *Mon. Wea. Rev.*, **123**, 1941–1963, https://doi.org/10.1175/1520-0493(1995)123<1941:TDKAME>2.0.CO;2.

Zagrodnik, J. P., and H. Jiang, 2014: Rainfall, convection, and latent heating distributions in rapidly intensifying tropical cyclones. *J. Atmos. Sci.*, **71**, 2789–2809, https://doi.org/10.1175/JAS-D-13-0314.1.

Zawislak, J., and Coauthors, 2022: Accomplishments of NOAA's airborne hurricane field program and a broader future approach to forecast improvement. *Bull. Amer. Meteor. Soc.*, **103**, E311–E338, https://doi.org/10.1175/BAMS-D-20-0174.1.

Zhang, F., and D. Tao, 2013: Effects of vertical wind shear on the predictability of tropical cyclones. *J. Atmos. Sci.*, **70**, 975–983, https://doi.org/10.1175/JAS-D-12-0133.1.

Zhang, J. A., R. F. Rogers, P. D. Reasor, and J. Gamache, 2023: The mean kinematic structure of the tropical cyclone boundary layer and its relationship to intensity change. *Mon. Wea. Rev.*, **151**, 63–84, https://doi.org/10.1175/MWR-D-21-0335.1.